Supplement of

Global simulation of semivolatile organic compounds – development and evaluation of the MESSy submodel SVOC (v1.0)

Mega Octaviani[1], **Holger Tost**[2], **Gerhard Lammel**[1,3,*]

[1]*Multiphase Chemistry Department, Max Planck Institute for Chemistry, 55128 Mainz, Germany*
[2]*Institute for Atmospheric Physics, Johannes Gutenberg University of Mainz, 55099 Mainz, Germany*
[3]*Research Centre for Toxic Compounds in the Environment, Masaryk University, 62500 Brno, Czech Republic*

[*]Correspondence to: g.lammel@mpic.de

Contents

SI Information used for ppLFER calculations **2**

SII Kinetic and physicochemical properties **5**

SIII Observation data screening **7**

SIV Factor separation technique **13**

SV Statistical indicators for model evaluation **14**

SVI Direct and interaction effects of factors on predicted near-surface PAH concentrations **16**

SVII Effects of all factors combination on model performance **34**

SVIII Spatial distribution of model bias **41**

SIX SVOC evaluation: Intermodel comparison **45**

Bibliography **49**

SI Information used for ppLFER calculations

Table S1. Gas−particle partition coefficient for every sorption system in the ppLFER

System	Unit	Equation
NIST diesel soot−air	$m^3_{air}\ m^{-2}_{surface}$	$\log_{10} K_{EC} = lL + aA + bB + c$
$(NH_4)_2SO_4$−air	$m^3_{air}\ m^{-2}_{surface}$	$\log_{10} K_{(NH_4)_2SO_4} = lL + aA + bB + c$
NaCl−air	$m^3_{air}\ m^{-2}_{surface}$	$\log_{10} K_{NaCl} = lL + aA + bB + c$
Dry DMSO−air	$L_{air}\ L^{-1}_{solvent}$	$\log_{10} K_{DMSO} = lL + sS + aA + bB + eE + c$
PU−air	$L_{air}\ kg^{-1}_{PU}$	$\log_{10} K_{PU} = lL + sS + aA + bB + vV + c$
Wet/dry hexadecane−air	$L_{air}\ L^{-1}_{solvent}$	$\log_{10} K_{hexadecane} = lL + sS + aA + bB + eE + c$

Table S2. ppLFER system parameters for gas−particle partition coefficients

System	e	s	a	b	v	l	c	T_0 (K)	Reference
NIST diesel soot−air	-	-	2.70	2.45	-	1.09	−8.47	288	Roth et al. (2005)
$(NH_4)_2SO_4$−air (20% RH)	-	-	2.46	5.23	-	0.90	−8.47	288	Goss et al. (2003)
$(NH_4)_2SO_4$−air (40% RH)	-	-	2.46	5.23	-	0.89	−8.47	288	Goss et al. (2003)
$(NH_4)_2SO_4$−air (60% RH)	-	-	2.13	5.34	-	0.88	−8.47	288	Goss et al. (2003)
NaCl−air (20% RH)	-	-	3.12	4.77	-	0.87	−8.47	288	Goss et al. (2003)
NaCl−air (40% RH)	-	-	2.94	4.82	-	0.86	−8.47	288	Goss et al. (2003)
NaCl−air (60% RH)	-	-	2.86	4.82	-	0.84	−8.47	288	Goss et al. (2003)
Dry DMSO−air	−0.22	2.90	5.04	0.00	-	0.72	−0.56	298	Abraham et al. (2010)
PU−air	-	1.69	3.66	0.00	0.36	0.71	−0.15	288	Kamprad and Goss (2007)
Wet/dry hexadecane−air	0.00	0.00	0.00	0.00	-	1.00	0.00	298	Abraham et al. (2010)

Table S3. Enthalpy of phase transfer for every sorption system in the ppLFER scheme

System	Unit	Equation
NIST diesel soot−air	J mol^{-1}	$\Delta H1 = -\Delta H^*_{\mathrm{vap}}$
$(NH_4)_2SO_4$−air	J mol^{-1}	$\Delta H2 = (-10.2 \times \log_{10} K_{(NH_4)_2SO_4} - 89.6) \times 10^3$
NaCl−air	J mol^{-1}	$\Delta H3 = (-10.2 \times \log_{10} K_{\mathrm{NaCl}} - 89.6) \times 10^3$
Dry DMSO−air	J mol^{-1}	$\Delta H4 = (l'L + s'S + a'A + b'B + v'V + c') \times 10^3$
PU-air	J mol^{-1}	$\Delta H5 = (l'L + s'S + a'A + v'V + c') \times 10^3$
Dry hexadecane−air	J mol^{-1}	$\Delta H6 = (l'L + s'S + a'A + b'B + v'V + c') \times 10^3$

*ΔH_{vap} values are given in Table S6

Table S4. ppLFER system parameters for phase transfer enthalpy

System	e'	s'	a'	b'	v'	l'	c'	Reference
Dry DMSO−air	-	−19.04	−47.80	−5.52	−0.75	−6.19	−2.39	Mintz et al. (2008)
PU−air	-	−17.60	−46.60	-	−12.80	−4.30	2.70	Kamprad and Goss (2007)
Dry hexadecane−air	-	−3.20	−1.51	2.58	−10.86	−6.79	−2.97	Abraham et al. (2010)

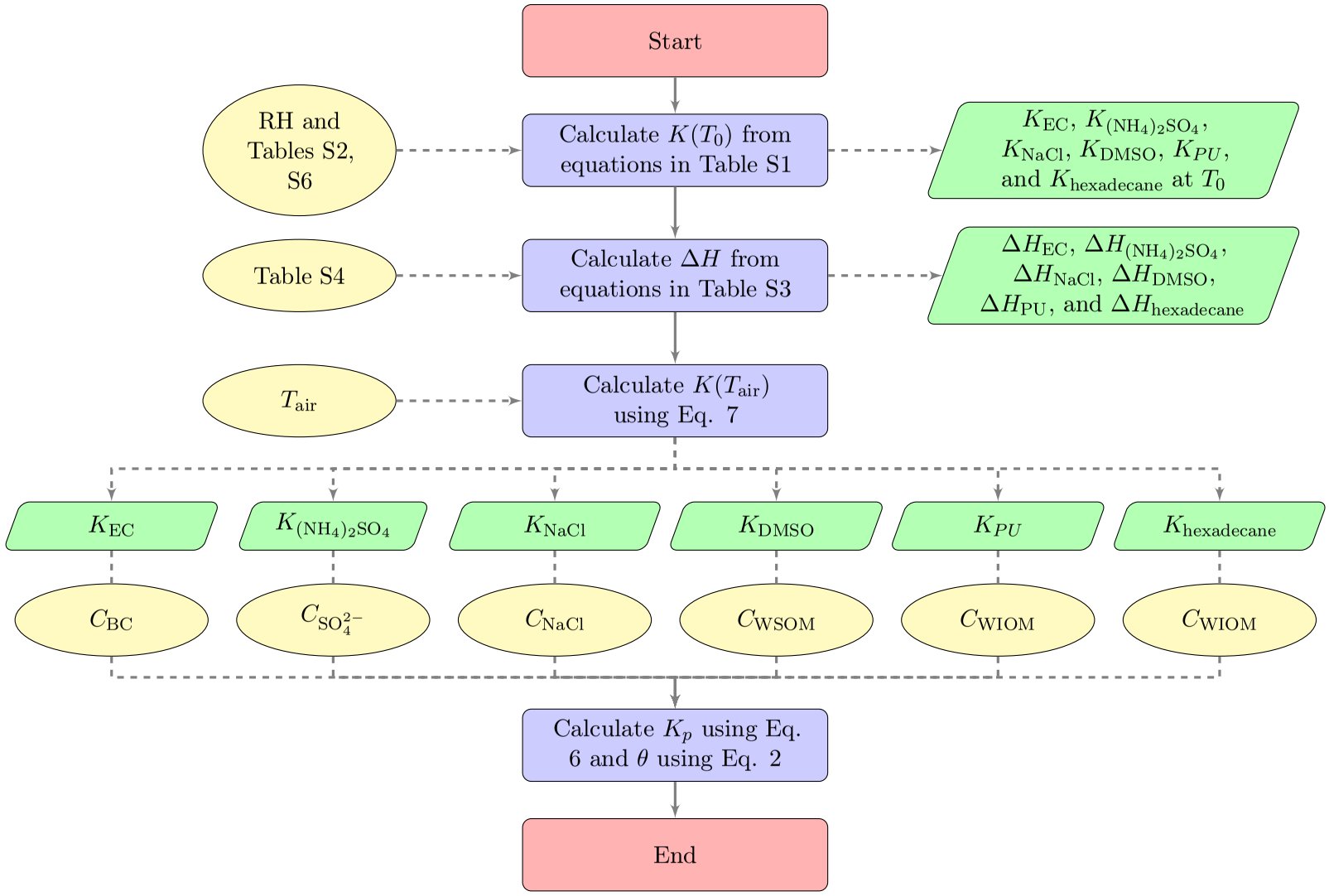

Figure S1. Schematic diagram in SVOC for the prediction of gas−particle partition coefficient using the ppLFER scheme

SII Kinetic and physicochemical properties

(Intentionally left blank)

Table S5. Physicochemical properties of selected PAHs

Parameter*	Unit	PHE	PYR	FLT	BaP	Reference
MW	g mol^{-1}	178.2	202.3	202.3	252.3	Finlayson-Pitts and Pitts (2000)
MV	cm^3 mol^{-1}	199.2	213.8	217.3	262.9	Mackay et al. (2006)
$k_{\mathrm{OH}}^{(2)}$	cm^3 molec^{-1} s^{-1}	2.7×10^{-11}[a]	5.0×10^{-11}[b]	1.1×10^{-11}[a]	-	[a]Brubaker and Hites (1998); [b]Finlayson-Pitts and Pitts (2000)
$k_{\mathrm{NO_3}}^{(2)}$	cm^3 molec^{-1} s^{-1}	1.2×10^{-13}	1.6×10^{-27} [NO_2]	5.1×10^{-28} [NO_2]	-	Finlayson-Pitts and Pitts (2000)
$k_{\mathrm{O_3}}^{(2)}$	cm^3 molec^{-1} s^{-1}	4.0×10^{-19}	-	-	-	Finlayson-Pitts and Pitts (2000)
$k_{\mathrm{O_3,het}}^{(2)}$	cm^3 molec^{-1} s^{-1}	$6.2\times10^{-17}\ \frac{S}{V}$	-	-	-	Perraudin et al. (2007)
$k_{\mathrm{O_3,het}}^{(1)}$	s^{-1}	-	-	-	$\frac{1.68\times10^{-16}}{(1/[O_3]+2.8\times10^{-15})}$	Kwamena et al. (2004)
k_{soil}	s^{-1}	5.17×10^{-7}	3.125×10^{-8}	2.08×10^{-8}	2.55×10^{-8}	Park et al. (1990)
k_{ocean}	s^{-1}	5.4×10^{-8}	2.8×10^{-9}	4.2×10^{-9}	1.3×10^{-9}	BioHCWin v1.01 (2008)
C_w^s	mg L^{-1}	1.10	0.132	0.26	0.0038	Finlayson-Pitts and Pitts (2000)
P_{sat}	Pa	7.0×10^{-2}[a]	6.0×10^{-4}[b]	1.24×10^{-3}[b]	1.22×10^{-5}[a]	[a]Yamasaki et al. (1984); [b]Wasik et al. (1983)
ΔH_{soln}	kJ mol^{-1}	34.81	35.44	39.83	50.6	Mackay et al. (2006)
ΔH_{vap}	kJ mol^{-1}	78.3	89.4	87.1	116.7	Roux et al. (2008)
ΔH_{subl}	kJ mol^{-1}	92.1	100.3	101.2	120.5	Roux et al. (2008)
$\log K_{\mathrm{ow}}$	-	4.47	5.01	4.97	6.05	Ma et al. (2010)
$K_{\mathrm{oa-m}}$	K	3293.[a]	3985.[b]	3904.[a]	5382.[a]	[a]Odabasi et al. (2006); [b]Harner and Bidleman (1998)
$K_{\mathrm{oa-b}}$	-	-3.37[a]	-4.56[b]	-4.34[a]	-6.50[a]	ibid.
$\mathrm{k_H^{\ominus}}$	M atm^{-1}	2.4×10^{1}[a]	5.9×10^{1}[a]	5.2×10^{1}[a]	2.2×10^{3}[b]	[a]Bamford et al. (1999); [b]ten Hulscher et al. (1992)
$\frac{\Delta H_{\mathrm{soln}}}{R}$	K	6000.[a]	5500.[a]	4900.[a]	4700.[b]	ibid.
ρ_{p}	kg m^{-3}	1174.	1271.	1252.	1351.	Mackay et al. (2006)

*Notes: MW: Molecular weight; MV: Molecular volume at boiling point; $k_{\mathrm{OH}}^{(2)}$: 2$^{\mathrm{nd}}$-order rate constant for gas-phase reaction with OH; $k_{\mathrm{NO_3}}^{(2)}$: 2$^{\mathrm{nd}}$-order rate constant for gas-phase reaction with NO_3; $k_{\mathrm{O_3}}^{(2)}$: 2$^{\mathrm{nd}}$-order rate constant for gas-phase reaction with O_3; $k_{\mathrm{O_3,het}}^{(2)}$: 2$^{\mathrm{nd}}$-order rate constant for heterogeneous oxidation with O_3; $k_{\mathrm{O_3,het}}^{(1)}$: Pseudo-1$^{\mathrm{st}}$-order rate constant for heterogeneous oxidation with O_3; $\frac{S}{V}$: Surface area of aerosols per unit volume of air (cm^2 cm^{-3}); k_{soil}: 1$^{\mathrm{st}}$-order rate constant for biotic and abiotic decay in soil; k_{ocean}: 1$^{\mathrm{st}}$-order rate constant for biotic and abitoc decay in ocean; C_w^s: Water solubility at 298.15 K; P_{sat}: Saturation vapor pressure at 298.15 K; ΔH_{soln}: Enthalpy of solution at 298.15 K; ΔH_{vap}: Enthalpy of vaporization at 298.15 K; ΔH_{subl}: Enthalpy of condensation of sub-cooled liquid at 298.15 K; K_{ow}: Octanol−water partition coefficient; K_{oa}: Temperature-dependent octanol−air partition coefficient; $\mathrm{k_H^{\ominus}}$: Henry's Law coefficient at 298.15 K; R: Gas constant (8.314 J mol^{-1} K^{-1}); ρ_{p}: Density of particulate-phase SOC.

Table S6. Abraham solute descriptors for selected PAHs

	E	*S*	*A*	*B*	*V*	*L*	Reference
PHE	1.92	1.28	0.00	0.29	1.45	7.71	Ariyasena and Poole (2014)
PYR	2.81	1.71	0.00	0.28	1.59	8.83	Sprunger et al. (2007)
FLT	2.38	1.55	0.00	0.24	1.59	8.83	Sprunger et al. (2007)
BaP	3.02	1.85	0.00	0.42	1.95	11.54	Ariyasena and Poole (2014)

SIII Observation data screening

Measured PAH concentration data have been collected from multiple monitoring networks (Table S7) where the locations of observation sites are distributed over the Arctic, mid-latitudes, and Tropics (Figure S2). Observations were used to assess the performance of the SVOC submodel to simulate total concentrations and particulate mass fraction, and to help select simulation period. For these purposes, the data were investigated carefully for suitability of use in this study using a sequence of data screening and quality checking illustrated in Figure S3. Tables S8 and S9 show the number of stations with reliable total concentration and particulate mass fraction data, respectively, for every PAH species and over each year from 2002 to 2014. It is found that the years 2007 to 2009 had sufficient quality-controlled data on the two variables, hence was deemed a suitable simulation period.

Table S7. Summary of observation networks for simulation period selection

Network	Data Availability	Variables	Reported Value	Data Source
EMEP & AMAP[a]	2002-2014	gas, particles, total	daily, weekly, monthly	EBAS NILU (2012)
DEFRA[b]	2008-2010	total	monthly	DEFRA (2010)
IADN[c]	2002-2010	gas, particles	daily	IADN (2014)
MONET-Africa[d]	2008	gas	monthly	Klánová et al. (2008)

[a] EMEP: European Monitoring and Environment Program; AMAP: Arctic Monitoring and Assessment Program
[b] DEFRA: Department for Environment, Food & Rural Affairs, UK
[c] IADN: Integrated Atmospheric Deposition Network
[d] MONET-Africa: The MONitoring NETtwork program in Africa

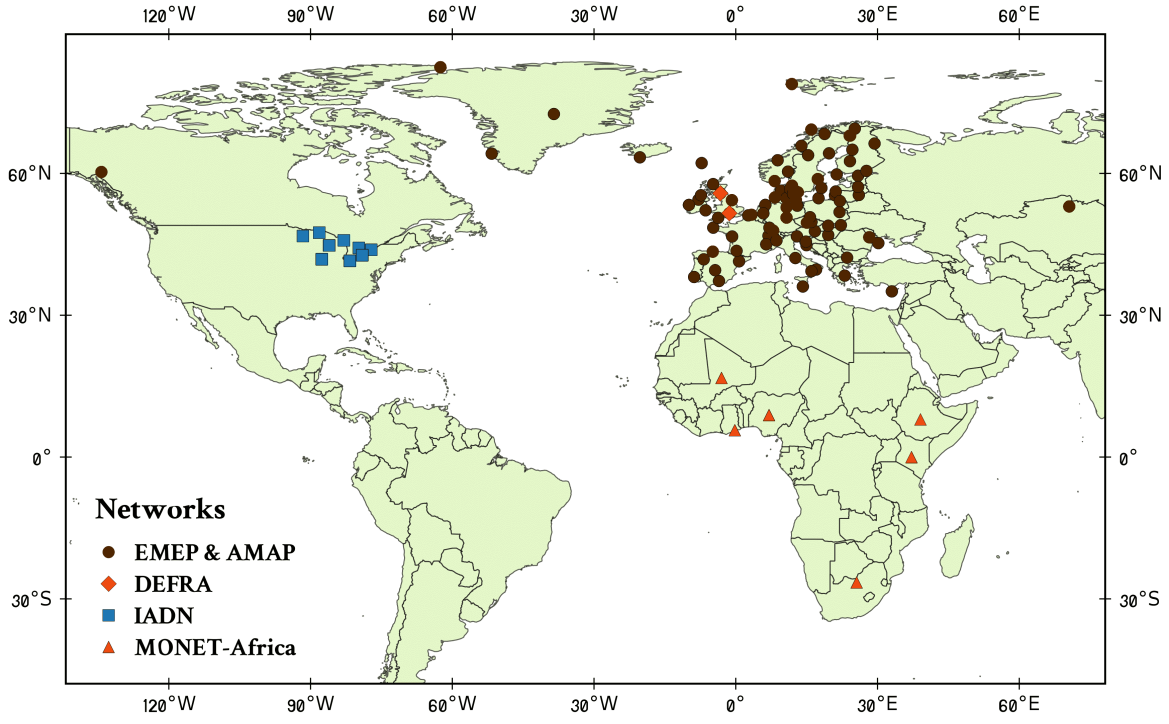

Figure S2. Available monitoring stations from all networks

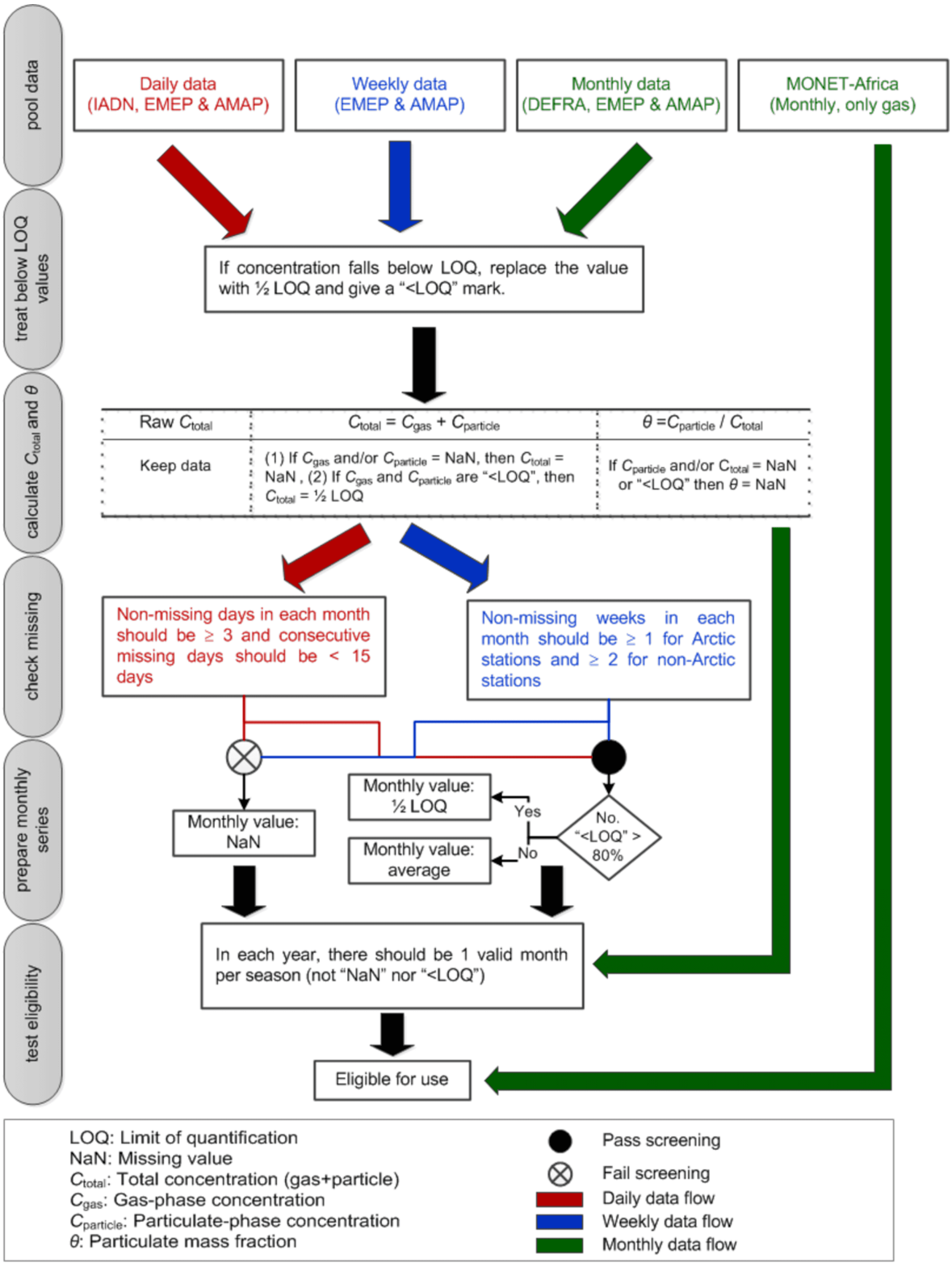

Figure S3. Flowchart of observation data screening and station selection strategy

Table S8. Number of stations each year that pass quality screening for total concentration data

	Network																			
	EMEP & AMAP				DEFRA				IADN				MONET-Africa			Total				
Year	PHE	PYR	FLT	BaP	PHE	PYR	FLT	BaP	PHE	PYR	FLT	BaP	PHE	PYR	FLT	PHE	PYR	FLT	BaP
2002	5	5	5	6	-	-	-	-	7	3	7	4	-	-	-	12	8	12	10
2003	5	5	5	5	-	-	-	-	7	3	7	4	-	-	-	12	8	12	9
2004	5	5	5	5	-	-	-	-	7	3	7	4	-	-	-	12	8	12	9
2005	5	5	5	5	-	-	-	-	6	3	6	3	-	-	-	11	8	11	8
2006	5	5	5	5	-	-	-	-	8	3	8	5	-	-	-	13	8	13	10
2007	9	9	9	10	-	-	-	-	7	2	7	7	-	-	-	16	11	16	17
2008	10	10	10	10	2	2	2	2	4	2	4	4	6	6	6	22	20	22	16
2009	8	10	9	10	2	2	2	2	5	2	5	5	-	-	-	15	14	16	17
2010	12	13	13	13	1	1	1	1	7	2	7	7	-	-	-	20	16	21	21
2011	5	9	6	6	-	-	-	-	-	-	-	-	-	-	-	5	9	6	6
2012	6	15	7	7	-	-	-	-	-	-	-	-	-	-	-	6	15	7	7
2013	9	10	10	10	-	-	-	-	-	-	-	-	-	-	-	9	10	10	10
2014	2	3	2	2	-	-	-	-	-	-	-	-	-	-	-	2	3	2	2

Table S9. Same as Table S8 but for particulate mass fraction

	Network											
	EMEP & AMAP				IADN				Total			
Year	PHE	PYR	FLT	BaP	PHE	PYR	FLT	BaP	PHE	PYR	FLT	BaP
2002	-	-	-	-	7	3	6	4	7	3	6	4
2003	-	-	-	-	6	3	7	4	6	3	7	4
2004	-	-	-	-	6	3	6	4	6	3	6	4
2005	-	-	-	-	6	3	6	3	6	3	6	3
2006	-	-	-	-	5	3	7	5	5	3	7	5
2007	1	1	1	1	4	2	5	7	5	3	6	8
2008	1	1	1	1	4	2	4	4	5	3	5	5
2009	-	-	-	-	4	2	4	5	4	2	4	5
2010	-	-	-	-	5	2	4	7	5	2	4	7

Table S10. List of final stations used in the model evalluation and the availability of monthly concentration data in each year

ID	Location	Lat.	Lon.	Data Availability		
				2007	2008	2009
			DEFRA[†]			
D1	Harwell, UK	51.6	−1.3	-	All	All
D2	Auchencorth Moss, UK	55.8	−3.2	-	All	All
			EMEP and AMAP[†]			
E1	Houtem, Belgium	51.3	3.4	-	-	PYR, FLT, BaP
E2	Alert, Canada	82.5	−62.5	All	All	All
E3	Kosetice, Czech Republic	49.6	15.1	All	All	All
E4	Westerland, Germany	54.9	8.3	All	All	All
E5	Schauinsland, Germany	47.9	7.9	All	All	All
E6	Schmücke, Germany	50.7	10.8	All	All	All
E7	Zingst, Germany	54.4	12.7	All	All	All
E8	Lahemaa, Estonia	59.5	25.9	BaP	BaP	BaP
E9	Pallas, Finland	24.2	68.0	All	All	-
E10	Birkenes, Norway	58.4	8.3	-	All	All
E11	Spitsbergen/Zeppelinfjell, Norway	78.9	11.9	All	PHE, PYR, FLT	All
E12	Aspvreten, Sweden	58.8	17.4	-	-	PYR
E13	Råö, Sweden	57.4	11.9	All	All	-
			IADN[†]			
I1	Burnt Island, Canada	45.8	−82.9	All	All	All
I2	Point Petre, Ontario Canada	43.8	−77.2	All	All	All
I3	Eagle Harbor, Michigan US	47.5	−88.1	PHE, FLT, BaP	-	PHE, FLT, BaP

continued . . .

Table S10: continued

ID	Location	Lat.	Lon.	Data Availability		
				2007	2008	2009
I4	IIT Chicago, Michigan US	41.8	−87.6	PHE, FLT, BaP	PHE, FLT, BaP	PHE, FLT, BaP
I5	Sleeping Bear Dunes, Michigan US	44.8	−86.1	PHE, FLT, BaP	-	PHE, FLT, BaP
I6	Sturgeon Point, New York US	42.7	−79.1	PHE, FLT, BaP	-	-
I7	Cleveland, Ohio US	41.5	−81.7	PHE, FLT, BaP	PHE, FLT, BaP	-
	MONET-Africa[‡,§]					
M1	Asela, Ethiopia	7.9	39.1	-	PHE, PYR, FLT	-
M2	Kwabenya, Ghana	5.7	−0.2	-	PHE, PYR, FLT	-
M3	Mt. Kenya, Kenya	−0.03	37.2	-	PHE, PYR, FLT	-
M4	Tombouctou, Mali	16.7	−3.0	-	PHE, PYR, FLT	-
M5	Sheda, Nigeria	8.9	7.1	-	PHE, PYR, FLT	-
M6	Molopo Nature Reserve, South Africa	−26.5	25.6	-	PHE, PYR, FLT	-

[†]Mid-latitude stations, except E2, E9, and E11 are the Arctic stations
[‡]Tropic stations
[§]Only concentration in the gas phase

Table S11. Same as Table S10 but for monthly particulate mass fraction data

	Data Availability		
Station ID	**2007**	**2008**	**2009**
E3	All	All	-
I1	All	All	All
I2	All	All	All
I3	BaP	-	BaP
I4	-	FLT	FLT
I5	FLT, BaP	-	FLT, BaP
I6	FLT, BaP	-	-
I7	FLT, BaP	FLT, BaP	-

SIV Factor separation technique

The factor separation (FS) analysis is introduced by Stein and Alpert (1993) to assess the contributions of each factor, as well as interactions among factors, to a particular output variable. This method has been applied in many numerical studies (e.g. Romero et al., 1997; Carvalho et al., 2006; Lynn et al., 2009; Torma and Giorgi, 2014) and is employed here to quantify the sensitivity of total concentration to changes in emission and physics parameterizations selected above. Following Stein and Alpert (1993), the effects of individual and interactive/synergistic changes are defined by:

$$\hat{f}_1 = f_1 - f_0 \tag{1a}$$
$$\hat{f}_2 = f_2 - f_0 \tag{1b}$$
$$\hat{f}_3 = f_3 - f_0 \tag{1c}$$
$$\hat{f}_4 = f_4 - f_0 \tag{1d}$$

$$\hat{f}_{12} = f_{12} - (f_1 + f_2) + f_0 \tag{2a}$$
$$\hat{f}_{13} = f_{13} - (f_1 + f_3) + f_0 \tag{2b}$$
$$\hat{f}_{14} = f_{14} - (f_1 + f_4) + f_0 \tag{2c}$$
$$\hat{f}_{23} = f_{23} - (f_2 + f_3) + f_0 \tag{2d}$$
$$\hat{f}_{24} = f_{24} - (f_2 + f_4) + f_0 \tag{2e}$$
$$\hat{f}_{34} = f_{12} - (f_3 + f_4) + f_0 \tag{2f}$$

$$\hat{f}_{123} = f_{123} - (f_{12} + f_{13} + f_{23}) + (f_1 + f_2 + f_3) - f_0 \tag{3a}$$
$$\hat{f}_{134} = f_{134} - (f_{13} + f_{14} + f_{34}) + (f_1 + f_3 + f_4) - f_0 \tag{3b}$$
$$\hat{f}_{124} = f_{124} - (f_{12} + f_{14} + f_{24}) + (f_1 + f_2 + f_4) - f_0 \tag{3c}$$
$$\hat{f}_{234} = f_{234} - (f_{23} + f_{34} + f_{24}) + (f_2 + f_3 + f_4) - f_0 \tag{3d}$$

$$\begin{aligned}\hat{f}_{1234} =& f_{1234} - (f_{134} + f_{134} + f_{124} + f_{234}) + \\ & (f_{12} + f_{13} + f_{14} + f_{23} + f_{24} + f_{34}) - \\ & (f_1 + f_2 + f_3 + f_4) + f_0\end{aligned} \tag{4}$$

where f_0 is the concentrations from a *base* simulation, $\hat{f}_1$ is the concentration changes influenced directly by the 1$^{\text{st}}$ factor (in this study is the temporal emission variation), $\hat{f}_2$ is by the 2$^{\text{nd}}$ factor (particulate-phase representation), $\hat{f}_3$ is by the 3$^{\text{rd}}$ factor (the choice of gas−particle partitioning scheme), and $\hat{f}_4$ is by the 4$^{\text{th}}$ factor (volatilization). $\hat{f}_{ij}$ gives information related to the non-linear interaction of 2 factors together (i and j) on the concentrations, $\hat{f}_{ijk}$ is from 3-factor interactions, and $\hat{f}_{1234}$ is from all factor interactions.

In this study, we have chosen to focus on interpreting the direct effects of individual factor ($\hat{f}_i$) and the effects of total interactions between the corresponding factor and all other factors ($\sum_j \hat{f}_{ij} + \sum_{j,k} \hat{f}_{ijk} + \hat{f}_{1234}$, $j \neq k \neq i$). Our main aims are to see if the interactions have the effects of strengthening or buffering the direct effects and examine the magnitude of the interactions relative to its associated direct effects.

SV Statistical indicators for model evaluation

Multiple performance indicators were applied for model evaluation (see Table S12) and the inherent limitations of each were recognized. The first comparison is based on the descriptive statistics of both observed and predicted concentrations, represented by the arithmetic mean ($\overline{O}$ or $\overline{M}$), median (Q_{2O} or Q_{2M}) and standard deviation (SD_O or SD_M). The geometric mean (GM_O or GM_M) is additionally used considering the distribution of air pollutant concentrations is mostly close to log-normal; hence GM treats extreme high and low equally.

Following the works of Chang and Hanna (2004), Yu et al. (2006), Galarneau et al. (2014) and many others, the simulation-to-observation comparison focuses on the mean bias (MB), root mean square error (RMSE), normalized mean bias (NMB), normalized mean bias factor (NMBF), fractions of predictions within a factor of 2 or 10 of observations (FAC2 and FAC10, respectively), and correlation coefficient (r). MB describes a general tendency of bias, but individual positive and negative errors tend to compensate each other. RMSE helps characterize the spread of individual bias and indicate any large outliers. Relative measures in NMB and NMBF are useful to compare the model performance for different substances in which concentrations can be largely different. The normalization of the difference in NMB leads to an asymmetry problem, that is, overpredictions are artificially unbounded whereas underpredictions are bounded by -100%. To overcome this issue, the study adopted NMBF introduced by Yu et al. (2006) by which the index is defined individually when $\overline{M} \geq \overline{O}$ and when $\overline{O} \leq \overline{M}$. It is also easy to interpret the index. If NMBF is positive (negative), the model overestimates (underestimates) the observations by a factor of NMBF $+1$ ($1 -$ NBMF). For example, if NMBF $= -2$, the model underestimates by a factor of 3. The last parameters, FAC2 and FAC10, give a simple measure of scattering that is less influenced by outliers, whereas r reflects the linear relationship between two datasets.

Although all of the above measures were computed and examined, most of the discussions were based on selected indices for simplicity. Note that prior to the model evaluation, predicted values at the model grid were bilinearly interpolated to each station location.

Table S12. List of performance indicators used in model evaluation

Metrics	Formula*	Ideal Value	Range
Arithmetic mean	$\overline{x} = \frac{\sum_{i=1}^{N} x_i}{N}$	$\overline{M} = \overline{O}$	$[0, +\inf)$
Median	$\mathrm{Q2}_x = x_i$, where $i = \frac{(N+1)}{2}$	$\mathrm{Q2}_M = \mathrm{Q2}_O$	$[0, +\inf)$
Standard deviation	$\mathrm{SD}_x = \sqrt{\frac{1}{N}\sum_{i=1}^{N}(x_i - \overline{x})^2}$	$\mathrm{SD}_M = \mathrm{SD}_O$	$[0, +\inf)$
Geometric mean	$\mathrm{GM}_x = \left(\prod_{i=1}^{N} x_i\right)^{\frac{1}{N}} = \exp\left[\frac{1}{N}\sum_{i=1}^{N}\ln x_i\right]$	$\mathrm{GM}_M = \mathrm{GM}_O$	$[0, +\inf)$
Mean bias	$\mathrm{MB} = \frac{\sum_{i=1}^{N}(M_i - O_i)}{N}$	0.0	$\left[-\overline{O}, +\inf\right)$
Root mean square error	$\mathrm{RMSE} = \sqrt{\frac{\sum_{i=1}^{N}(M_i - O_i)^2}{N}}$	0.0	$[0, +\inf)$
Normalized mean bias	$\mathrm{NMB} = \frac{\mathrm{MB}}{\overline{O}} \times 100\%$	0.0	$[-100\%, +\inf)$
Normalized mean bias factor	$\mathrm{NMBF} = S\left[\exp\left(\left\lvert\ln\frac{\overline{M}}{\overline{O}}\right\rvert\right) - 1\right]$, where $S = \frac{\overline{M}-\overline{O}}{\lvert\overline{M}-\overline{O}\rvert}$	0.0	$(-\inf, +\inf)$
Factor of 2	$\mathrm{FAC2} = \frac{1}{N}\sum_{i=1}^{N} n_i$, with $n_i = \begin{cases} 1, & \text{if } 0.5 \le \frac{M_i}{O_i} \le 2 \\ 0, & \text{otherwise} \end{cases}$	1.0	$[0, 1]$
Factor of 10	$\mathrm{FAC10} = \frac{1}{N}\sum_{i=1}^{N} n_i$, with $n_i = \begin{cases} 1, & \text{if } 0.1 \le \frac{M_i}{O_i} \le 10 \\ 0, & \text{otherwise} \end{cases}$	1.0	$[0, 1]$
Correlation coefficient	$r = \frac{\sum_{i=1}^{N}\left(M_i - \overline{M}\right)\left(O_i - \overline{O}\right)}{\sqrt{\sum_{i=1}^{N}\left(M_i - \overline{M}\right)^2}\sqrt{\sum_{i=1}^{N}\left(O_i - \overline{O}\right)^2}}$	1.0	$[-1, 1]$

*Notes: x: Modeled/Simulated (M) or Observed (O) data; N: Number of monthly data or monthly pairs

SVI Direct and interaction effects of factors on predicted near-surface PAH concentrations

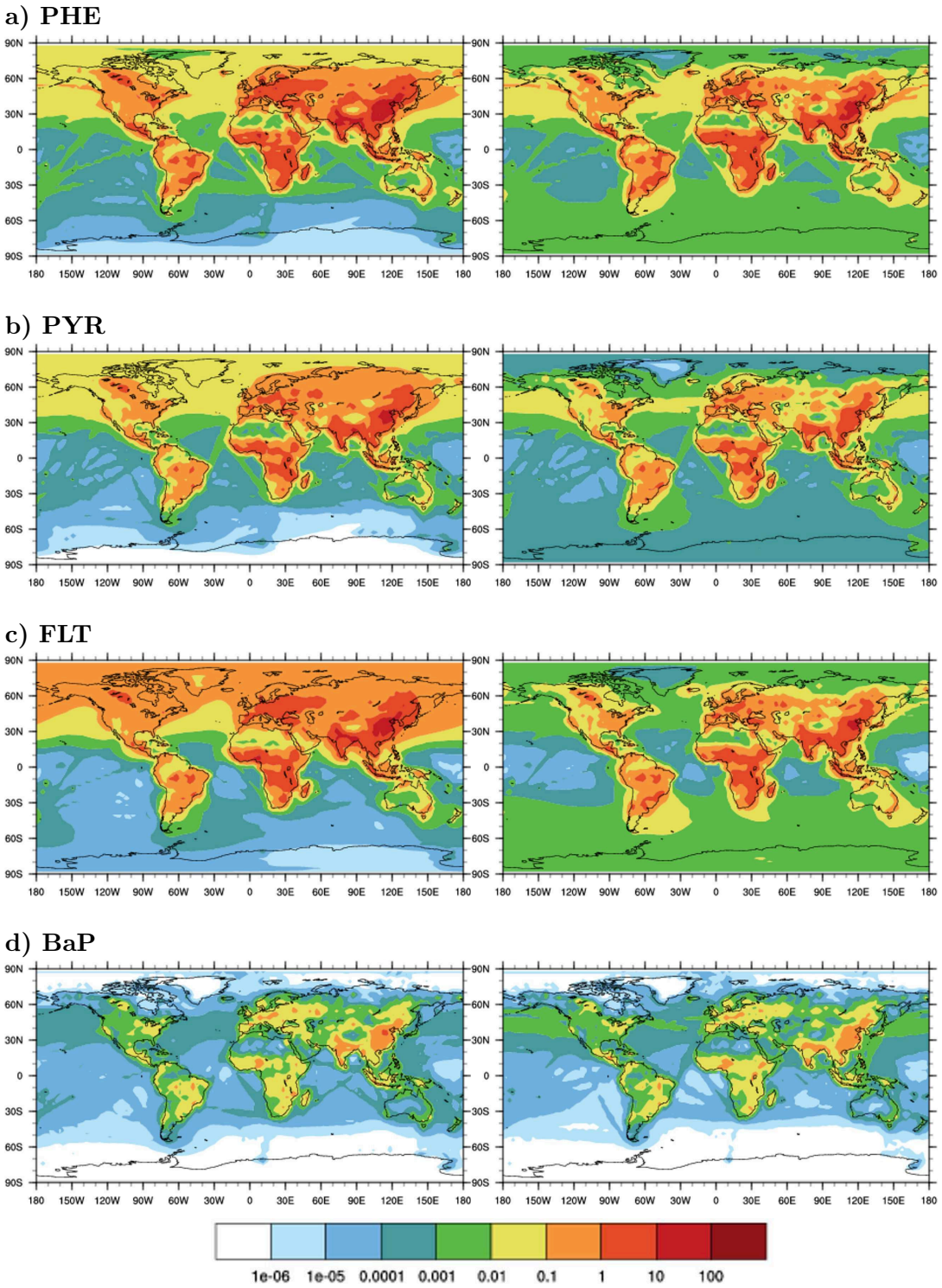

Figure S4. Seasonal mean near-surface PAH concentrations (ng m^{-3}) from the *base* simulation (f_0) for December–January–February (left panels) and June–July–August (right panels) 2007–2009. Here, f_0 represents a simulation applying annual emissions, the *bulk* scheme, the Lohmann–Lammel partitioning scheme, and no volatilization.

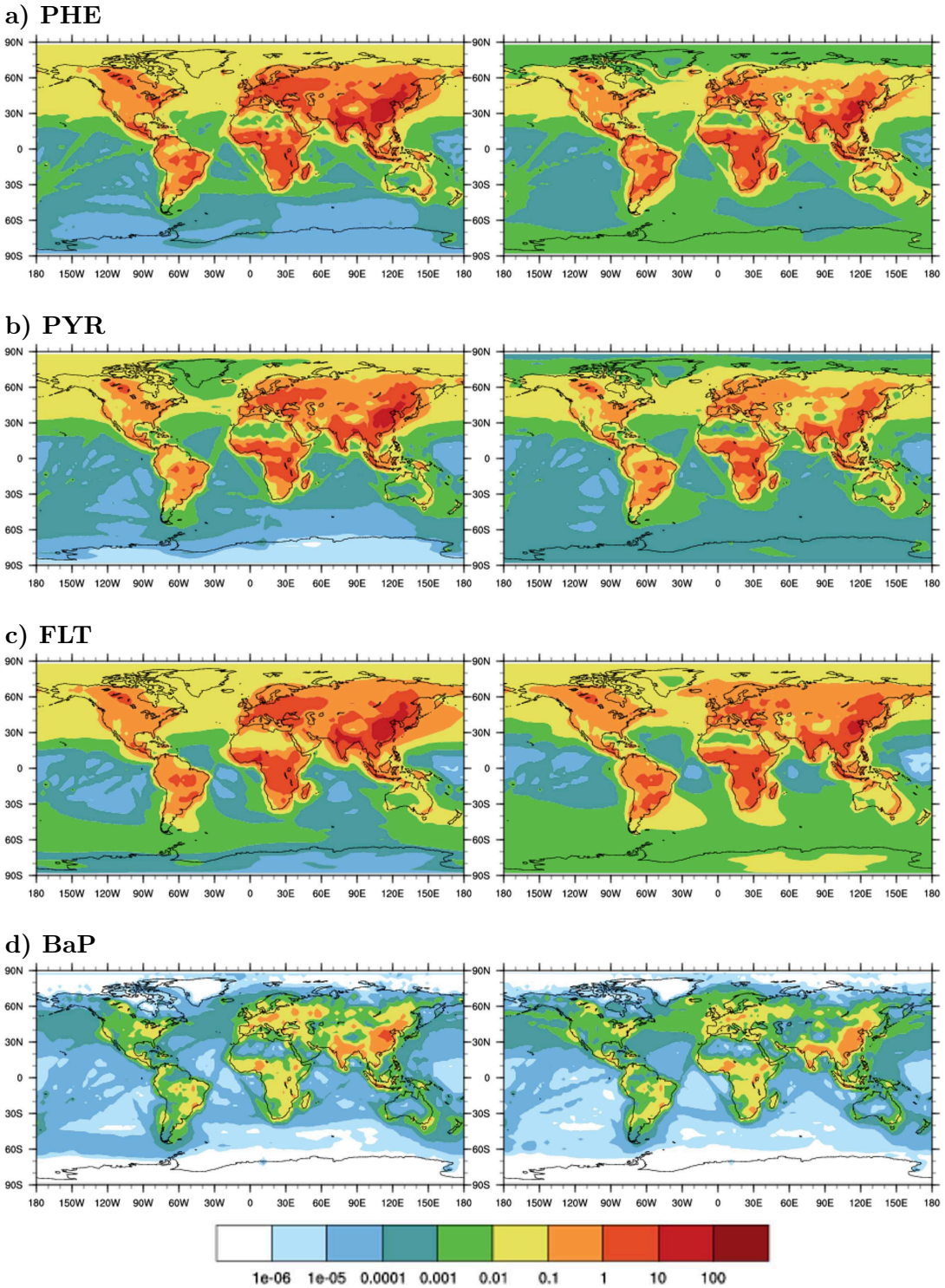

Figure S5. Same as Figure S4 but from the *target* simulation (f_{1234}). Here, f_{1234} represents a simulation applying seasonal emissions, the *modal* scheme, the ppLFER partitioning scheme, and with volatilization.

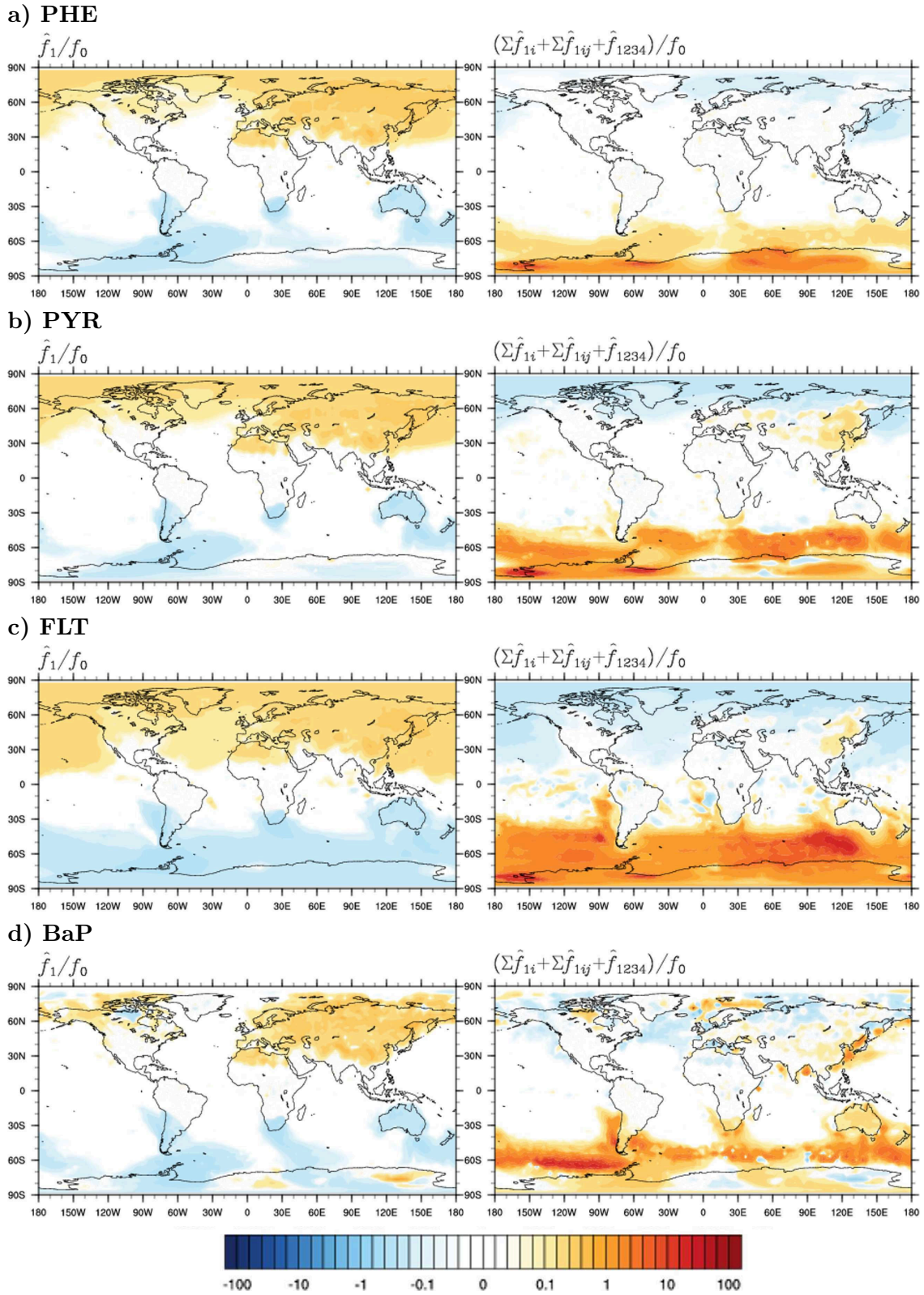

Figure S6. The effects of monthly emissions (in place of annual emissions) on near-surface PAH concentrations relative to concentrations from the base simulation (f_0), averaged over December–January–February 2007–2009: (left panels) direct effects ($\hat{f}_1$), expressed as the difference between two distributions: $\hat{f}_1 = f_1 - f_0$; (right panels) interaction effects, expressed as the sum of two ($\Sigma\hat{f}_{1j}$, $j \neq 1$), three ($\Sigma\hat{f}_{1jk}$, $j \neq k \neq 1$), and four ($\hat{f}_{1234}$) factor interactions.

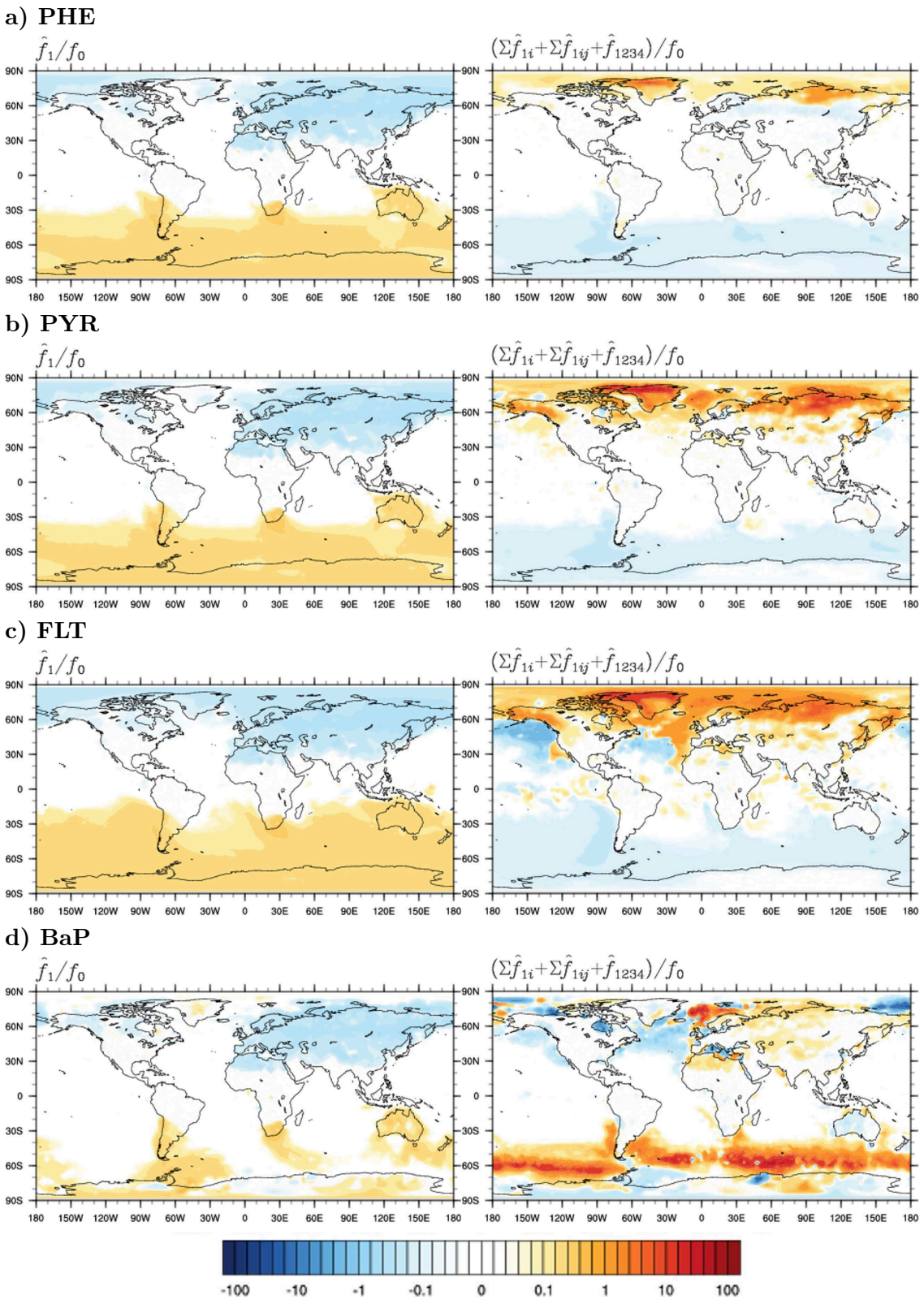

Figure S7. Same as Figure S6, but averaged over June–July–August 2007–2009

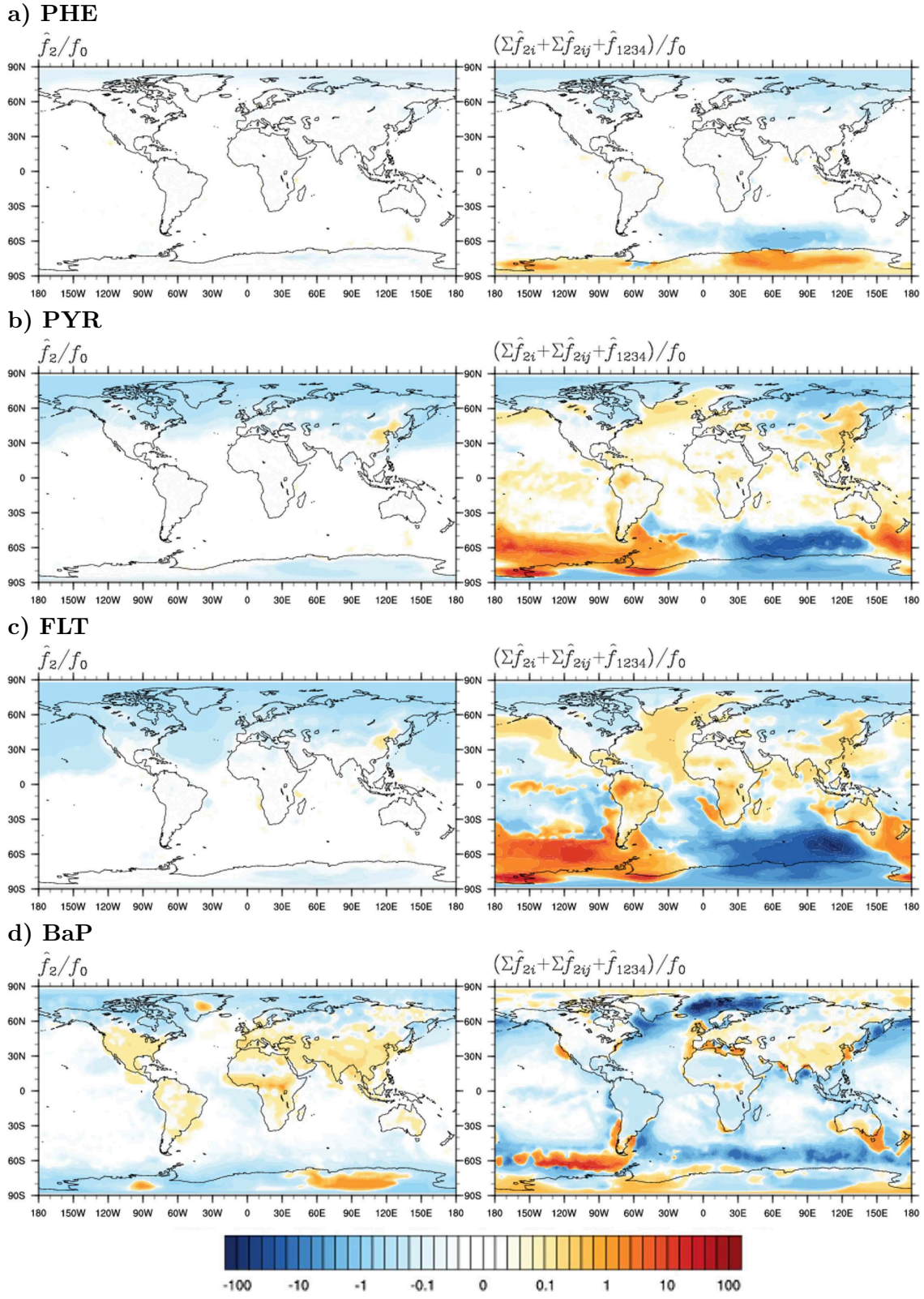

Figure S8. The effects of the *modal* scheme (in place of the *bulk* scheme) for particulate-phase representation on near-surface PAH concentrations relative to concentrations from the base simulation (f_0), averaged over December–January–February 2007–2009: (left panels) direct effects ($\hat{f}_2$), expressed as the difference between two distributions: $\hat{f}_2 = f_2 - f_0$; (right panels) interaction effects, expressed as the sum of two ($\Sigma\hat{f}_{2j}$, $j \neq 2$), three ($\Sigma\hat{f}_{2jk}$, $j \neq k \neq 2$), and four ($\hat{f}_{1234}$) factor interactions.

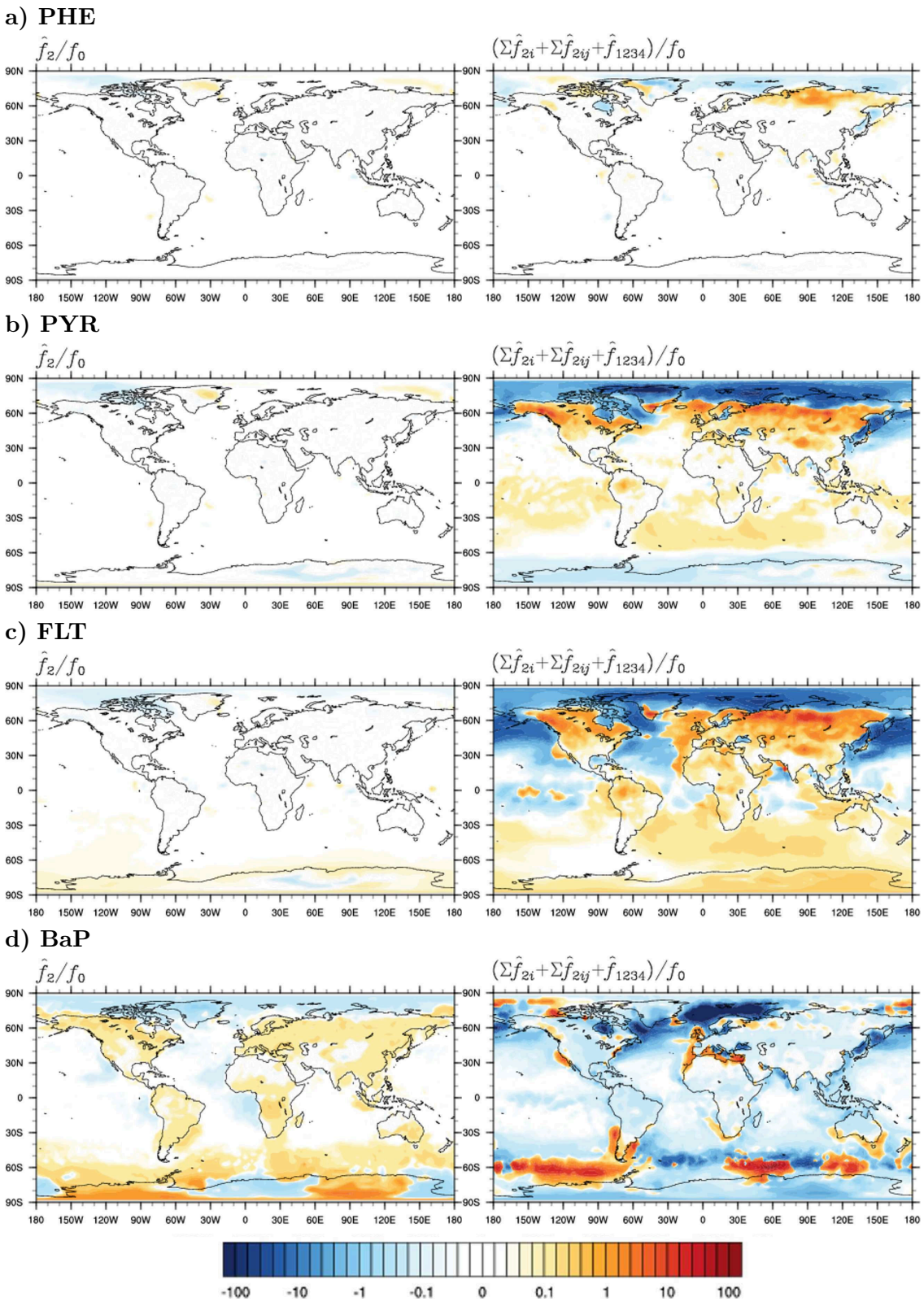

Figure S9. Same as Figure S8, but averaged over June–July–August 2007–2009

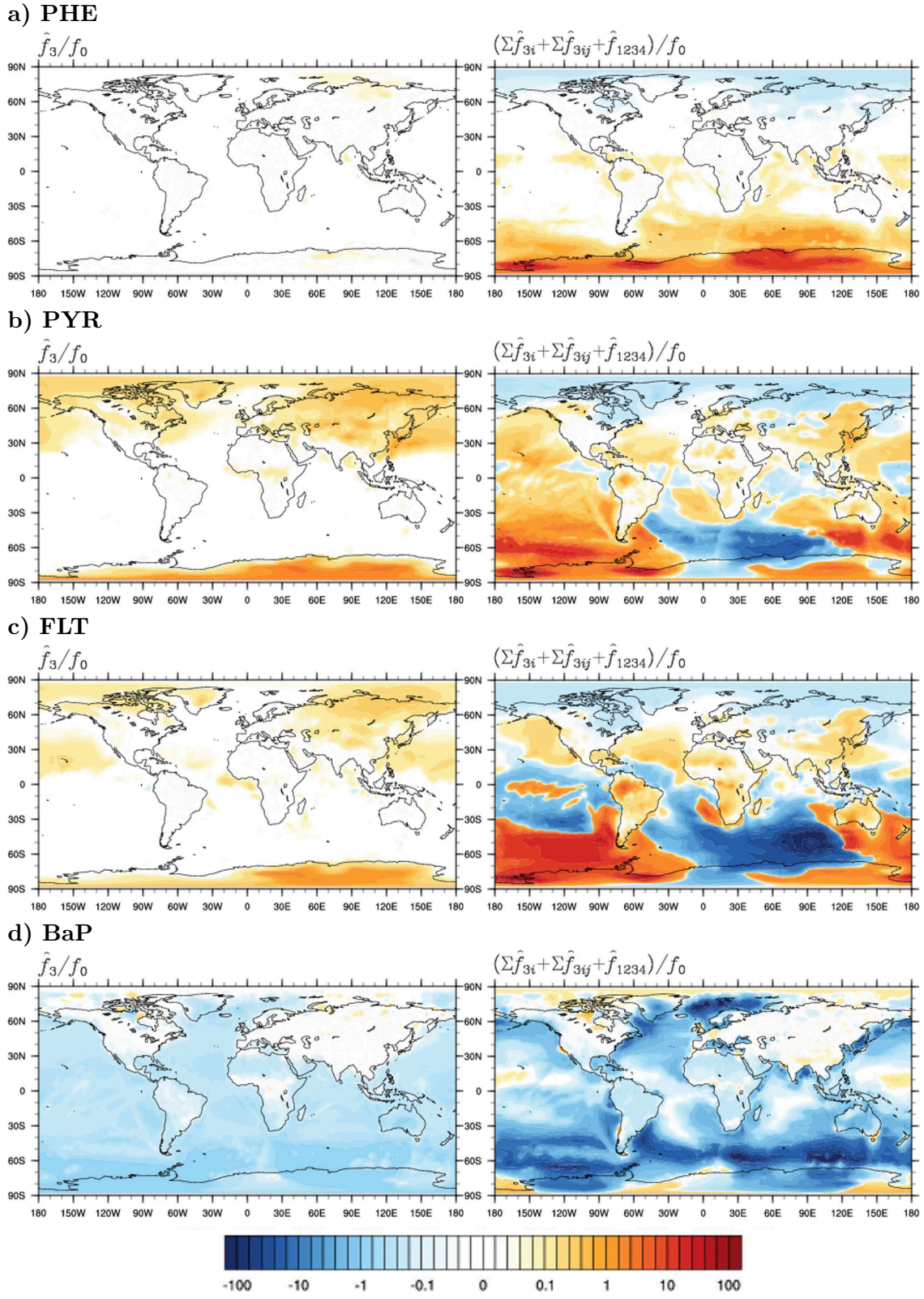

Figure S10. The effects of ppLFER scheme (in place of Lohmann–Lammel scheme) for gas–particle partitioning on near-surface PAH concentrations relative to concentrations from the base simulation (f_0), averaged over December–January–February 2007–2009: (left panels) direct effects ($\hat{f}_3$), expressed as the difference between two distributions: $\hat{f}_3 = f_3 - f_0$; (right panels) interaction effects, expressed as the sum of two ($\Sigma\hat{f}_{3j}$, $j \neq 3$), three ($\Sigma\hat{f}_{3jk}$, $j \neq k \neq 3$), and four ($\hat{f}_{1234}$) factor interactions.

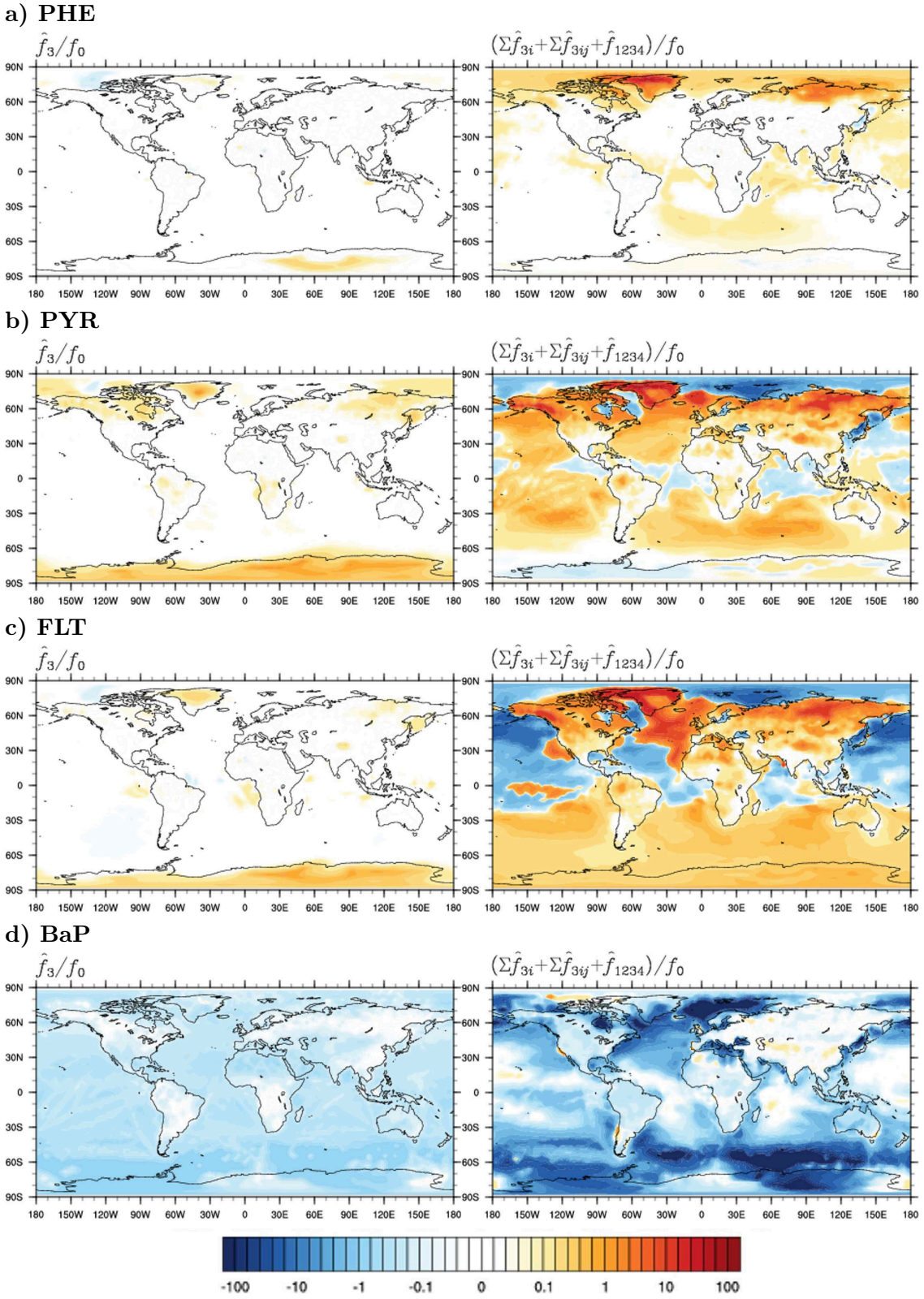

Figure S11. Same as Figure S10, but averaged over June–July–August 2007–2009

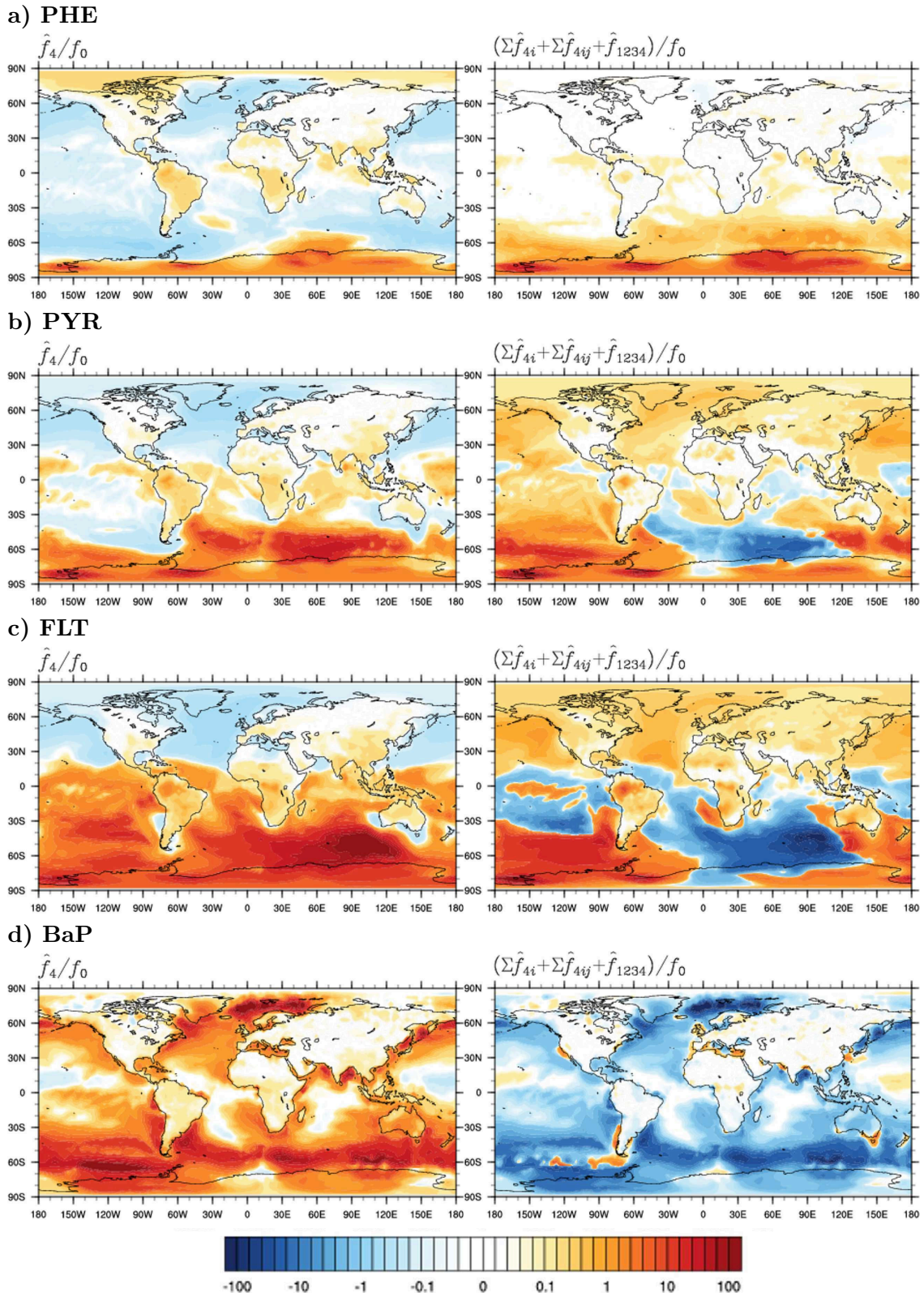

Figure S12. The effects of volatilization on near-surface PAH concentrations relative to concentrations from the base simulation (f_0), averaged over December–January–February 2007–2009: (left panels) direct effects ($\hat{f}_4$), expressed as the difference between two distributions: $\hat{f}_4 = f_4 - f_0$; (right panels) interaction effects, expressed as the sum of two ($\Sigma\hat{f}_{4j}$, $j \neq 4$), three ($\Sigma\hat{f}_{4jk}$, $j \neq k \neq 4$), and four ($\hat{f}_{1234}$) factor interactions.

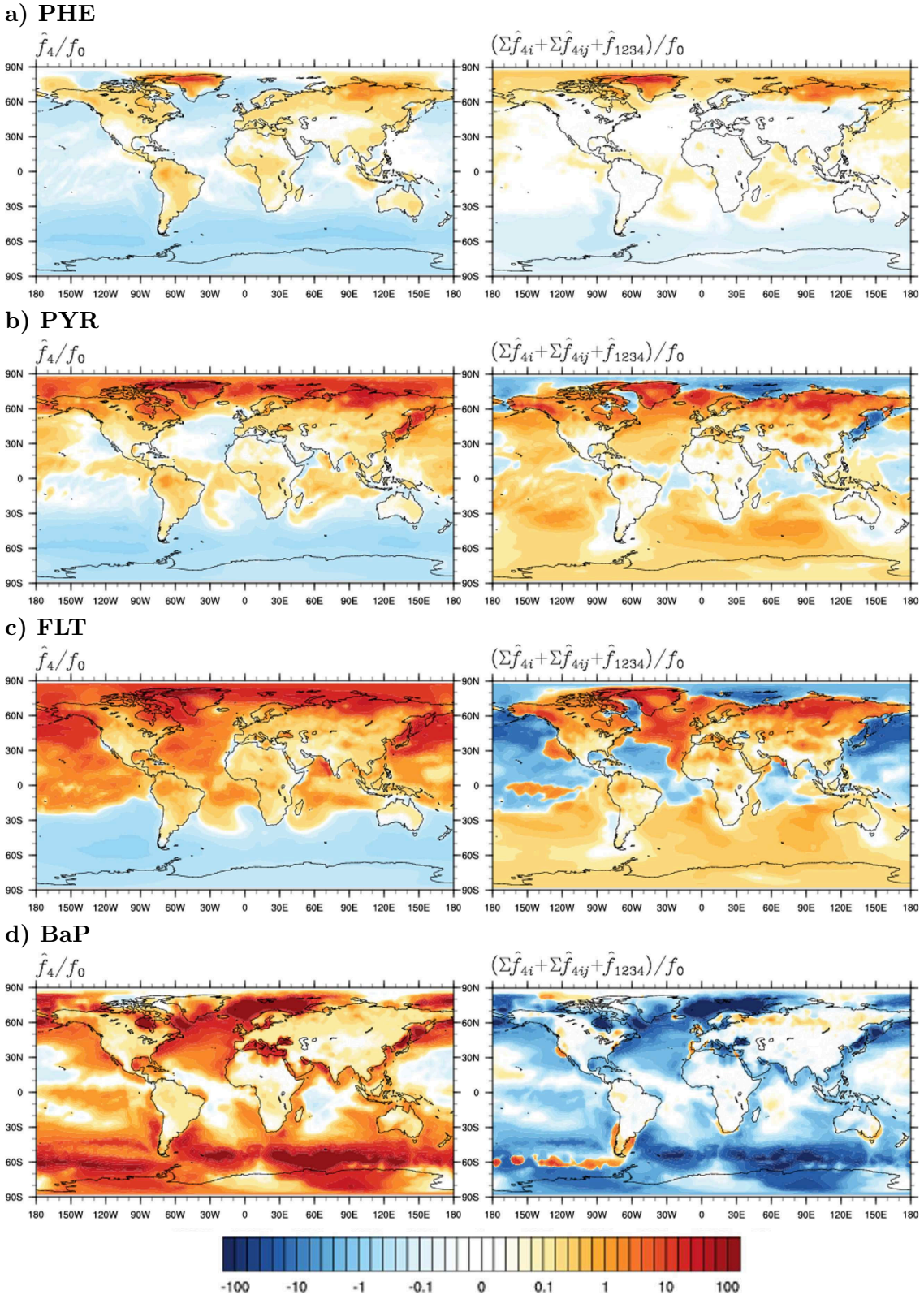

Figure S13. Same as Figure S12, but averaged over June–July–August 2007–2009

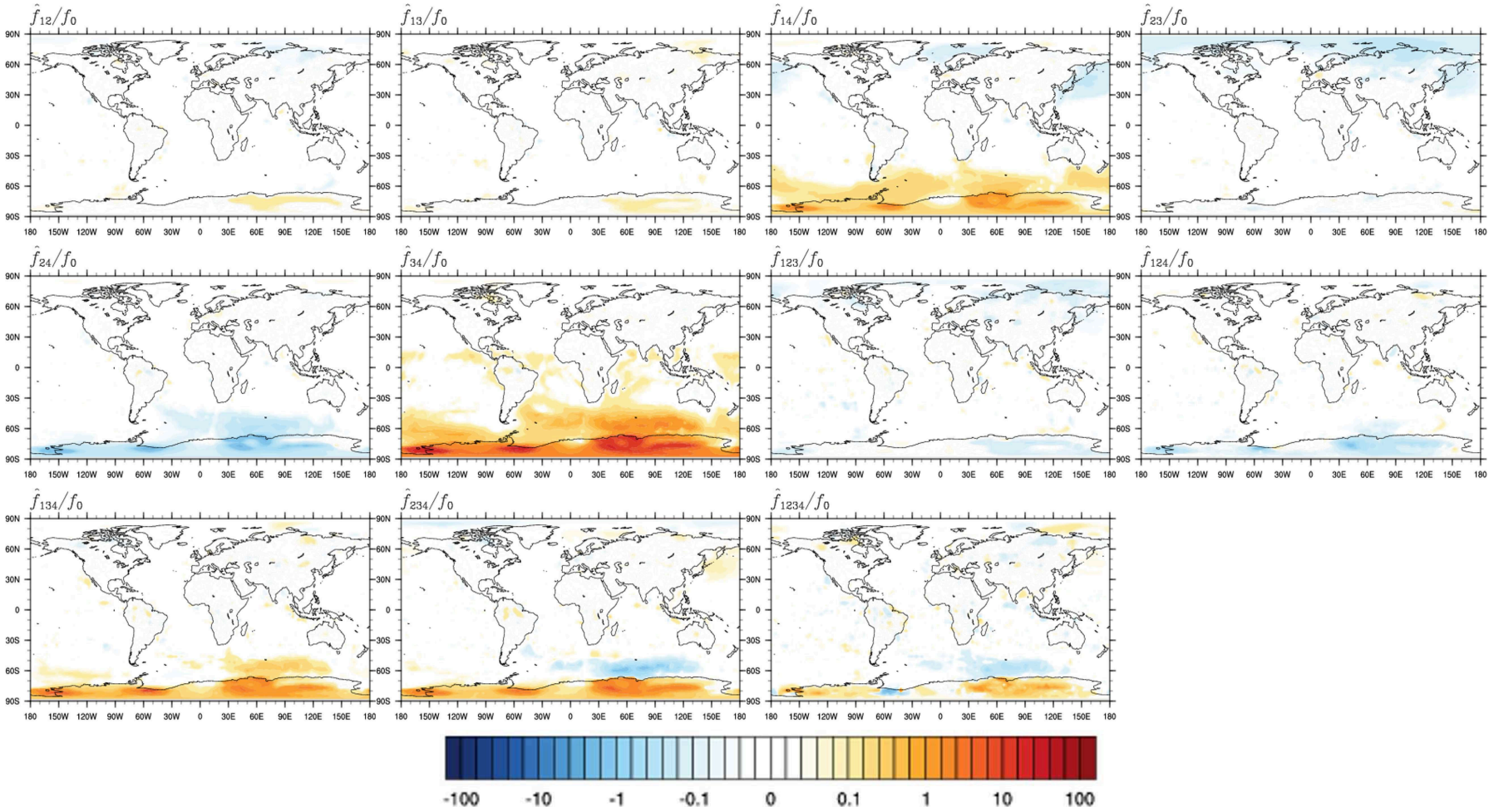

Figure S14. Average effects on near-surface PHE concentrations relative to concentrations from the base simulation (f_0) from interactions between two ($\hat{f}_{ij}$), three ($\hat{f}_{ijk}$), and four different factors ($\hat{f}_{1234}$); means of December–January–February 2007–2009.

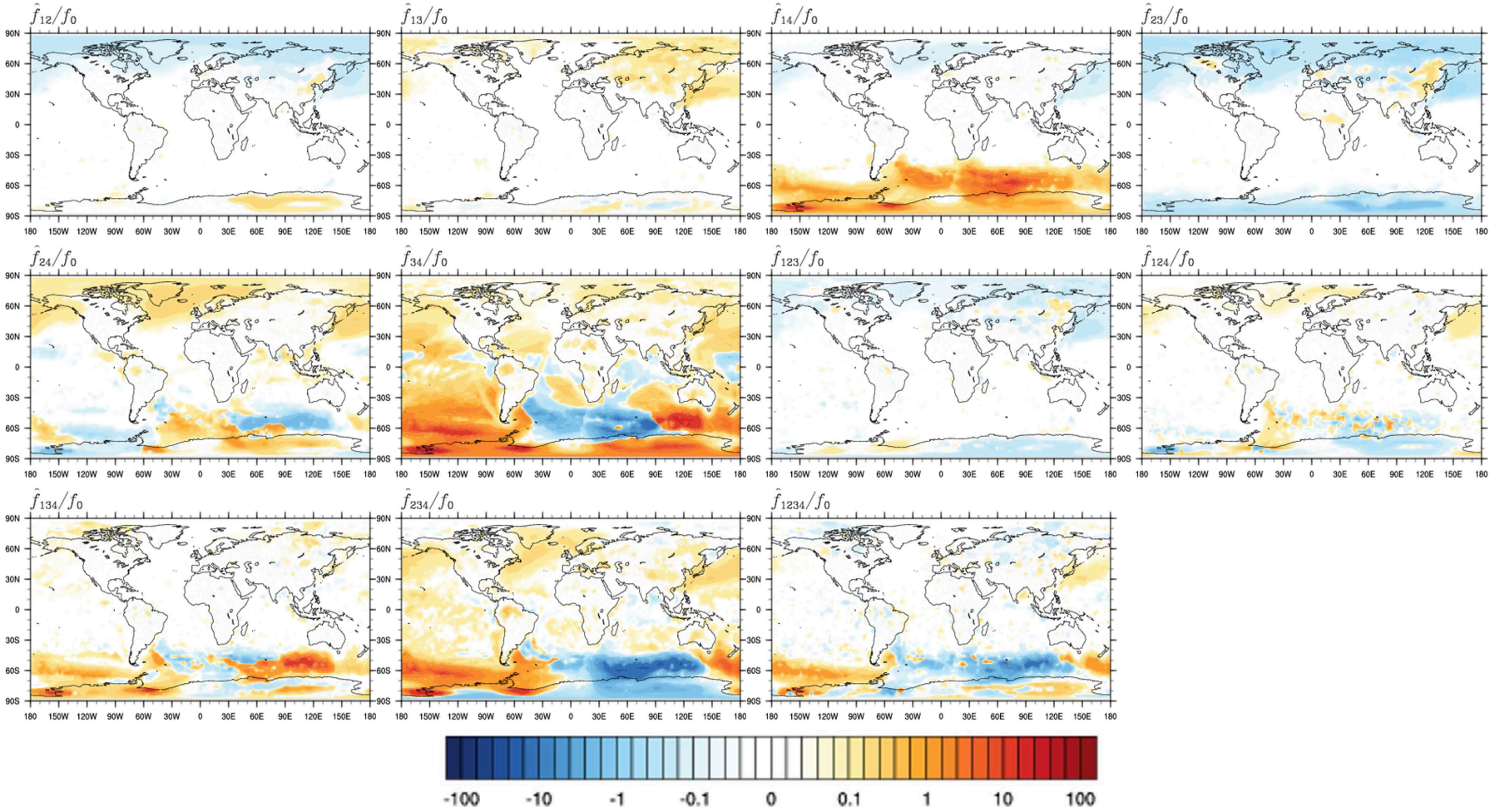

Figure S15. Same as Figure S14, but for PYR

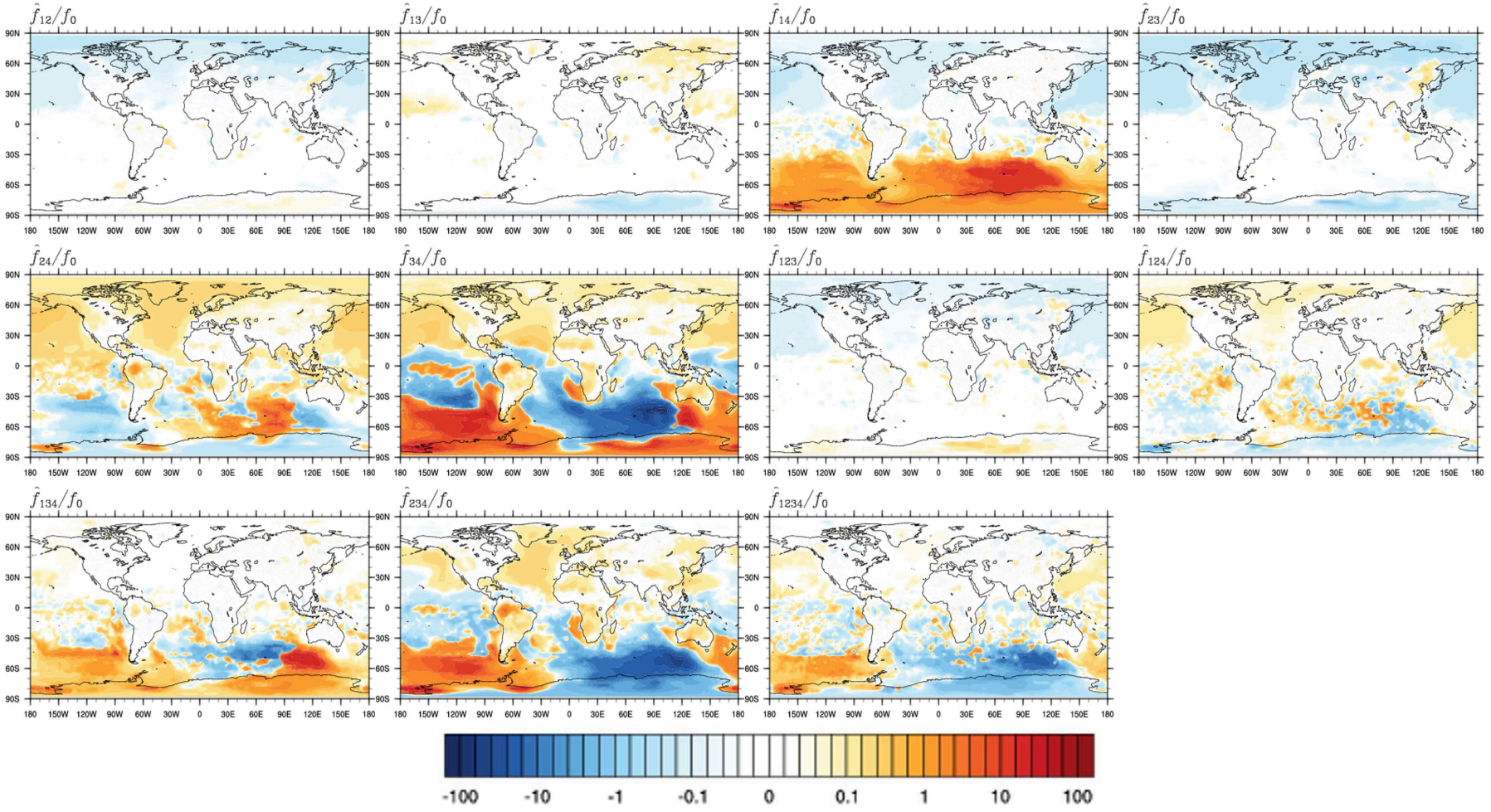

Figure S16. Same as Figure S14, but for FLT

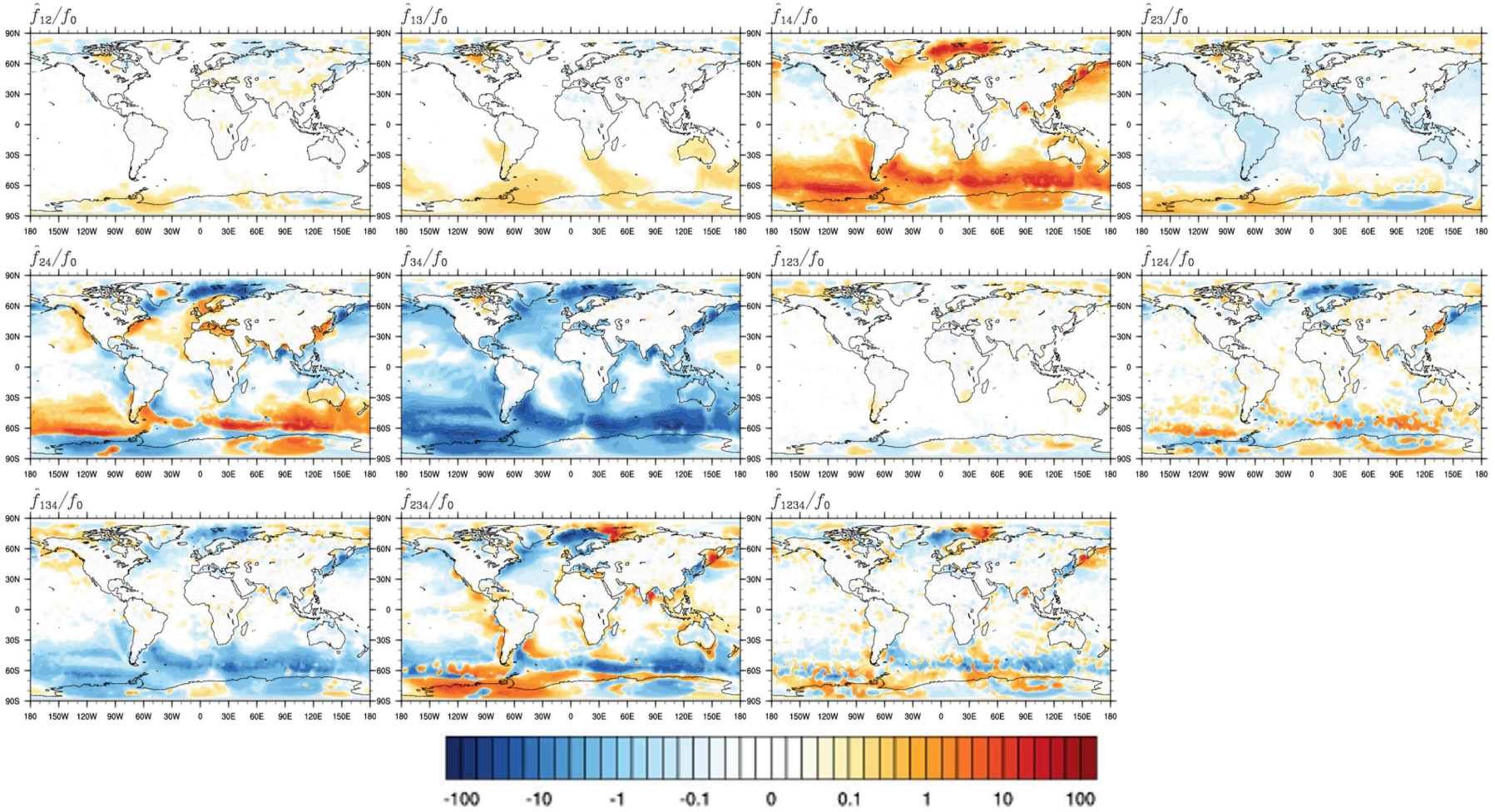

Figure S17. Same as Figure S14, but for BaP

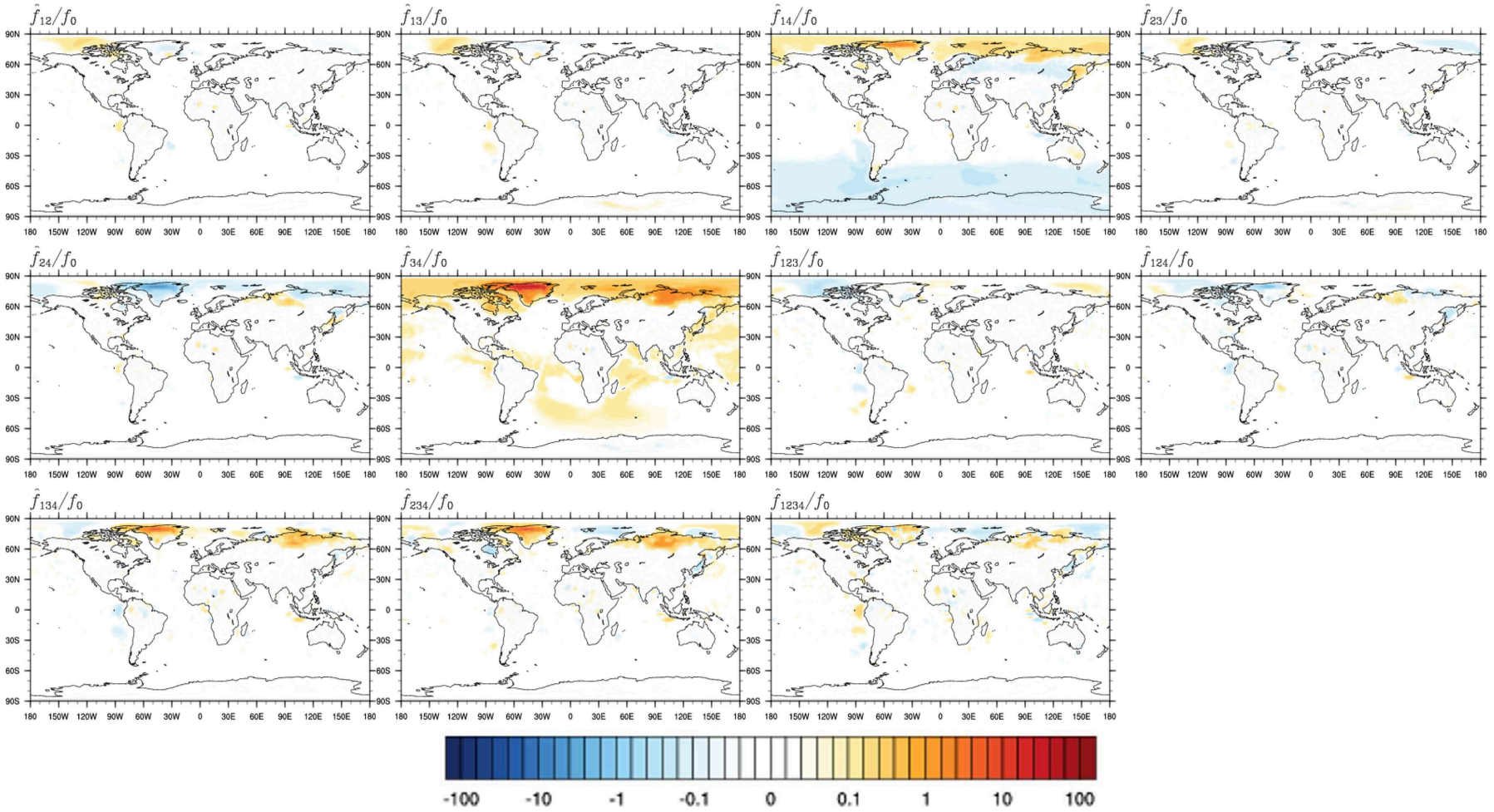

Figure S18. Average effects on near-surface PHE concentrations relative to concentrations from the base simulation (f_0) from interactions between two ($\hat{f}_{ij}$), three ($\hat{f}_{ijk}$), and four different factors ($\hat{f}_{1234}$); means of June–July–August 2007–2009.

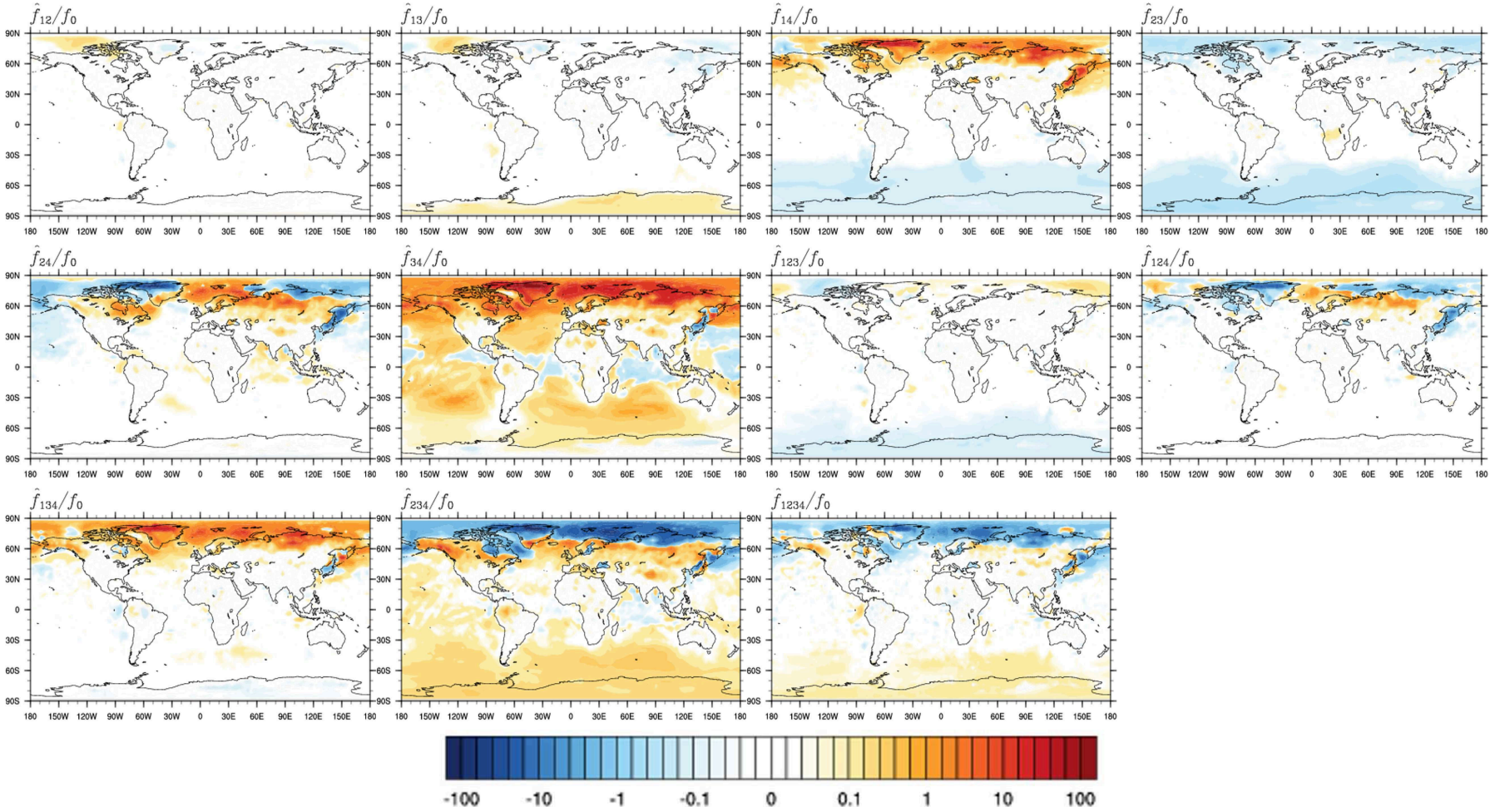

Figure S19. Same as Figure S18, but for PYR

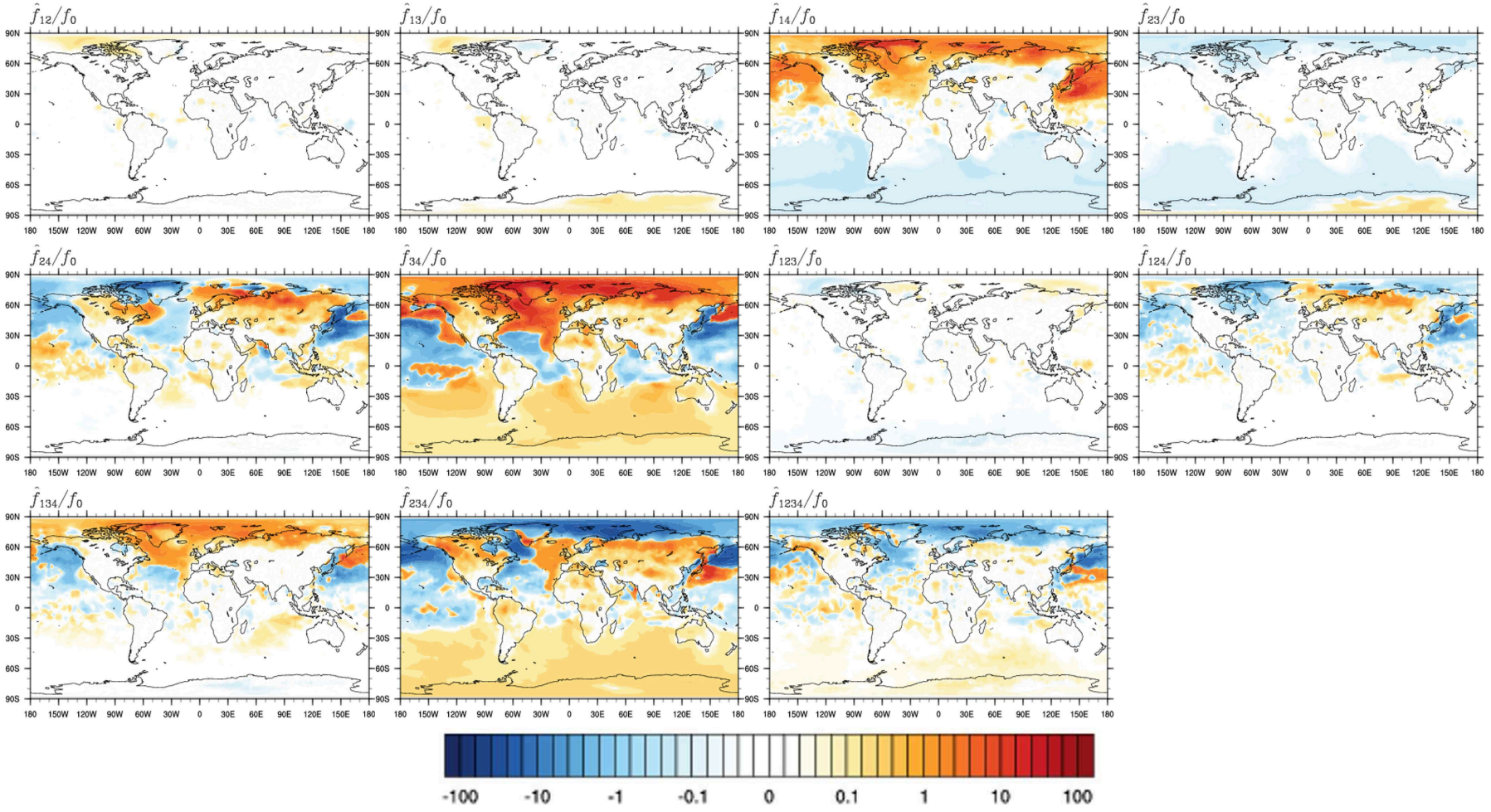

Figure S20. Same as Figure S18, but for FLT

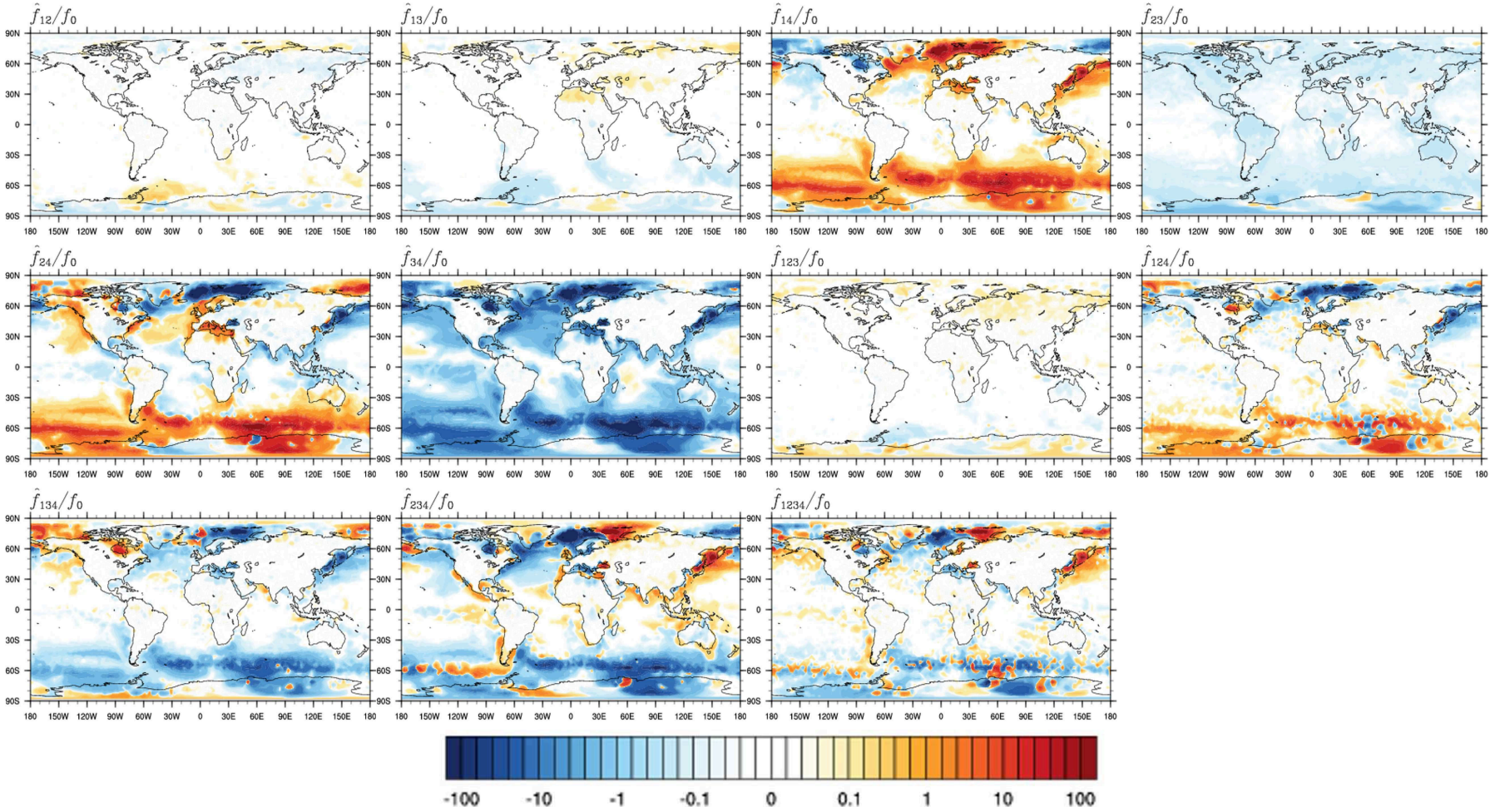

Figure S21. Same as Figure S18, but for BaP

SVII Effects of all factors combination on model performance

In the following, simulated outputs from 16 sensitivity experiments are compared against observation data for two seasons (DJF and JJA) and two regions (Arctic and NH mid-latitudes). Note that while results from factor separation analysis express the effects of each selected factor (see Sect. SIV) relative to a reference (i.e., f_0), the discussion below focuses on how the factors affect the model performance in general. Here, the mean concentration difference (hereinafter, ΔConc) across all possible combinations of two experiments is used, where only one of the four factors is different between the two experiments. For example, the effect of emission seasonality (*fac1*) will be represented as mean of SBLN − ABLN, SBLW − ABLW, SBPN − ABPN, SBPW − ABPW, SMLN − AMLN, SMLW − AMLW, SMPN − AMPN, and SMPW − AMPW (refer to Figure 3 of the Main text for the acronyms). Note that if the mean difference from the first four pairs is different with that from the last four, it indicates that the *fac1* interaction with *fac2* (particulate-phase representation) plays an important role in the model performance.

Phenanthrene

Figure S22 displays the seasonal mean values and mean bias (MB) of PHE concentrations averaged across monitoring stations in the Arctic and NH mid-latitudes. As shown, all experiments underestimate the seasonal concentrations over the Arctic, suggesting an inherent model bias. It is also apparent that the model is most sensitive to the change in emission interval (*fac1*). One can see that concentration increases in DJF (hence, MB improves) and decreases in JJA (hence, MB deteriorates) when monthly emission is applied in the simulations. This result is expected and is attributed to the seasonal cycle of emissions over NH. On average, ΔConc is 0.009 ng m^{-3} in DJF and −0.007 ng m^{-3} in JJA. Volatilization (*fac4*) appears as the second dominant factor as it contributes to decrease PHE concentrations in DJF and to increase them in JJA, an effect opposite to that of *fac1*. The degree of *fac4* effect is four times smaller than *fac1* effect, but they become comparable in JJA due to pronounced volatilization in boreal summer. The model performance is less sensitive to the choice of aerosol-phase treatment (*fac2*) and gas−particle partitioning scheme (*fac3*). Nevertheless, it is found that the *modal* scheme enhances the underestimation in DJF when it interacts with the ppLFER scheme ($\Delta\text{Conc}_{\text{DJF}} = -0.003$ to -0.005 ng m^{-3}).

For the northern mid-latitudes, the model response is still dominated by the change in *fac1*, followed by the change in *fac4*. Due to proximity to emission sources, the response to monthly emissions is stronger than that found for the Arctic, i.e., 0.127 ng m^{-3} in DJF and −0.330 ng m^{-3} in JJA. The emission change also brings model predictions closer to observations. As for volatilization, its effect is positive (concentration increases) in both seasons (on average, $\Delta\text{Conc}_{\text{DJF}} = 0.066$ and $\Delta\text{Conc}_{\text{JJA}} = 0.300$ ng m^{-3}), which leads to a smaller underestimation in DJF and a higher overestimation in JJA. The effects of alternating *fac2* and *fac3* are small-to-negligible, particularly during the summer months. This finding is somewhat expected given the fact that smaller aerosol fraction of the most-volatile PAH in

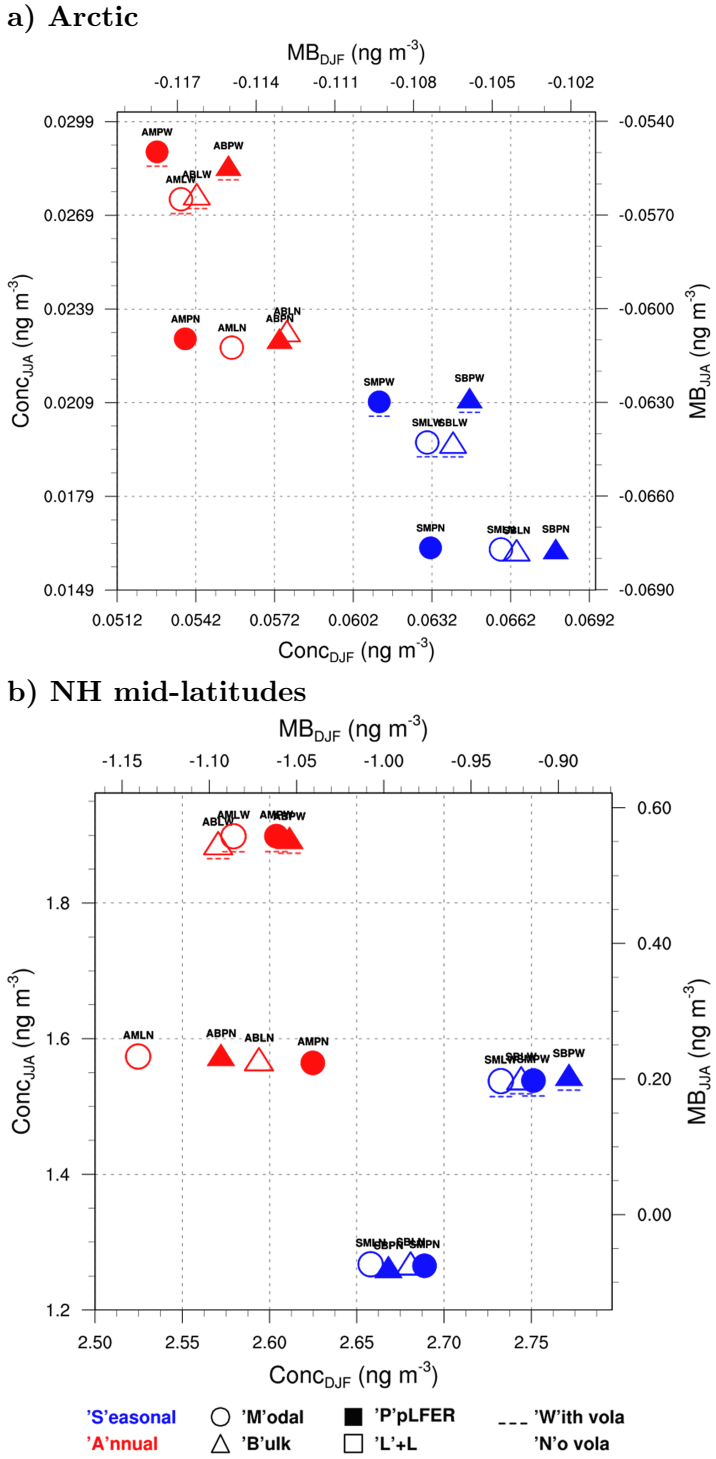

Figure S22. Seasonal mean PHE concentrations and mean bias (MB) from 16 sensitivity experiments, averaged across stations in the a) Arctic and b) northern mid-latitudes. Changes in color represent the change in emission interval (*fac1*), changes in shape represent the change in particulate-phase representation (*fac2*), and changes in shape fill represent the change in gas–particle partitioning scheme (*fac3*). Symbols with a dashed line refer to model experiments with volatilization (*fac4*).

summer coincides with an increase in temperature which increases the vapor pressure of the compound and decreases the gas−particle partition coefficient.

Pyrene

The effects of individual factor on PYR concentrations over the Arctic were found to vary by season (Figure S23a). In DJF, the largest contribution to concentration differences between experiments comes from the choice of *fac2*. In particular, the *modal* scheme decreases the concentrations ($\Delta\text{Conc}_{\text{DJF}} = -0.025$ to -0.073 ng m^{-3}) and produces negative biases. The effects of monthly emissions and volatilization are comparable but of opposite signs, being positive for the former and overall negative for the latter. Compared to *fac2* effect, the concentration differences imposed by both factor changes are smaller by nearly a factor of two in the *bulk*-scheme scenario and by around a factor of six in the *modal*-scheme scenario. The influence *fac3* depends on the selected *fac2* because only in the *bulk* (*modal*) scheme scenario is there a positive (negative) response to the ppLFER scheme. Turning now to JJA, the results suggest that volatilization has a positive effect on predicted PYR concentrations, with an average increase being 0.016 ng m^{-3}, and results in positive model biases. The effects of *fac2* and *fac3* changes are very small but become apparent when volatilization is applied. Specifically, using the *modal* scheme increases JJA concentrations by 0.004 ng m^{-3} whereas the ppLFER scheme brings an increase of 0.009 ng m^{-3}, thereby enhancing the overestimation. Also in JJA, the model performance is least sensitive to the change in emission interval.

In Figure S23b it is shown that all experiments overestimate PYR concentrations over NH mid-latitudes in both seasons. The differences in predictions are most by the positive effect of volatilization which magnifies the overestimation. Here, the average concentration increase is 0.124 ng m^{-3} in DJF and twice that in JJA. The effect of ppLFER scheme is also positive and tends to be stronger when volatilization is applied (on average, $\Delta\text{Conc}_{\text{DJF}} = 0.106$ ng m^{-3} and $\Delta\text{Conc}_{\text{JJA}} = 0.062$ ng m^{-3}). Seasonal emission increases concentrations in DJF (0.053 ng m^{-3}) but decreases those in JJA (-0.142 ng m^{-3}). The *modal* scheme tends to show the opposite, that is, a decrease in DJF and an increase in JJA with an average response in both seasons being 0.030 ng m^{-3}.

Fluoranthene

PYR and FLT share some similarities as further discussed below. Figure S24a shows that *fac2* effect is dominant on Arctic concentrations in DJF. In particular, the *modal* scheme decreases the simulated concentrations (on average, $\Delta\text{Conc}_{\text{DJF}} = -0.124$ ng m^{-3}) and improves MB. The opposite (positive) signal is expected from monthly emissions and volatilization, with mean $\Delta\text{Conc}_{\text{DJF}}$ being 0.020 ng m^{-3} and 0.045 ng m^{-3}, respectively. The ppLFER scheme leads to a concentration decrease (-0.034 ng m^{-3}), indicating shorter lifetime, except when in combination with the *bulk* scheme and volatilization. In JJA, the positive effect of volatilization prevails and becomes dominant (on average, $\Delta\text{Conc}_{\text{JJA}} = 0.072$ ng m^{-3}) and the experiments produce a systematic positive bias. The change in gas−particle partitioning scheme yields

a) Arctic

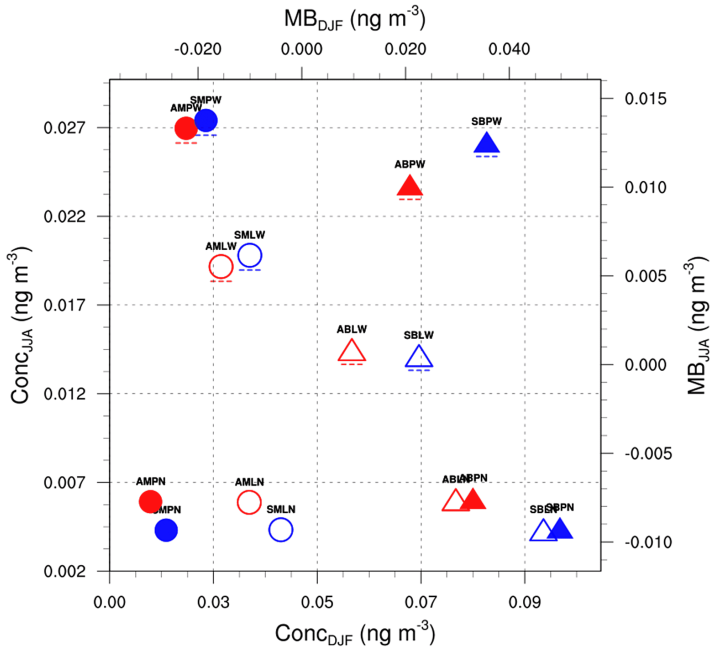

b) NH mid-latitudes

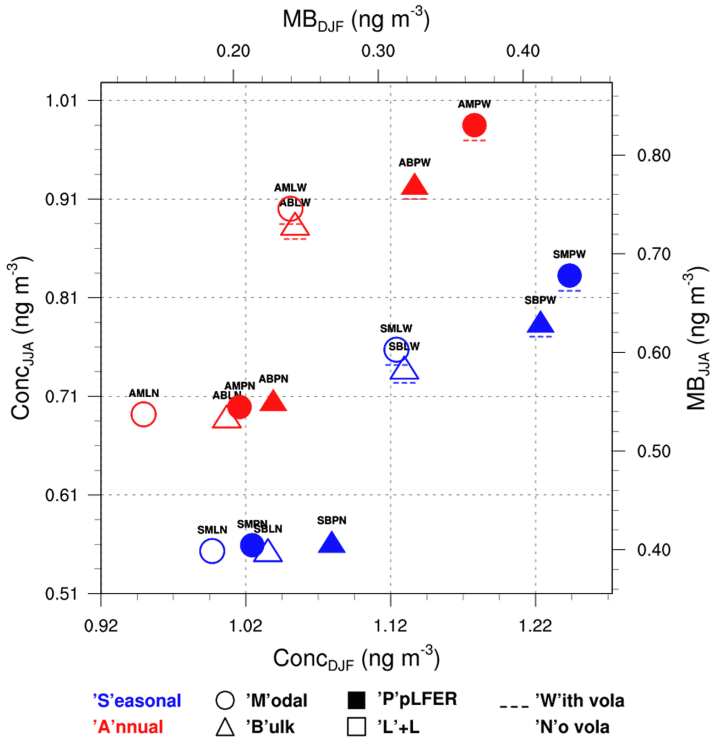

Figure S23. Same as Figure S22, but for PYR concentrations

a) Arctic

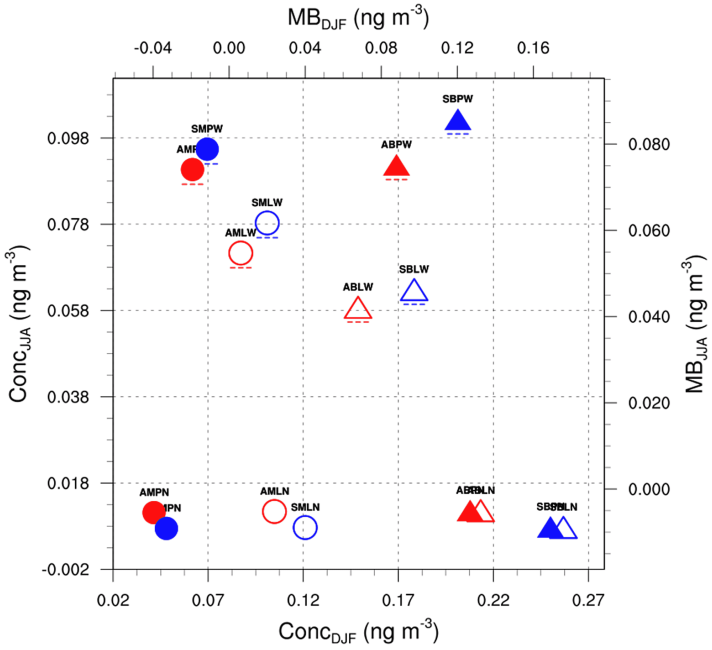

b) NH mid-latitudes

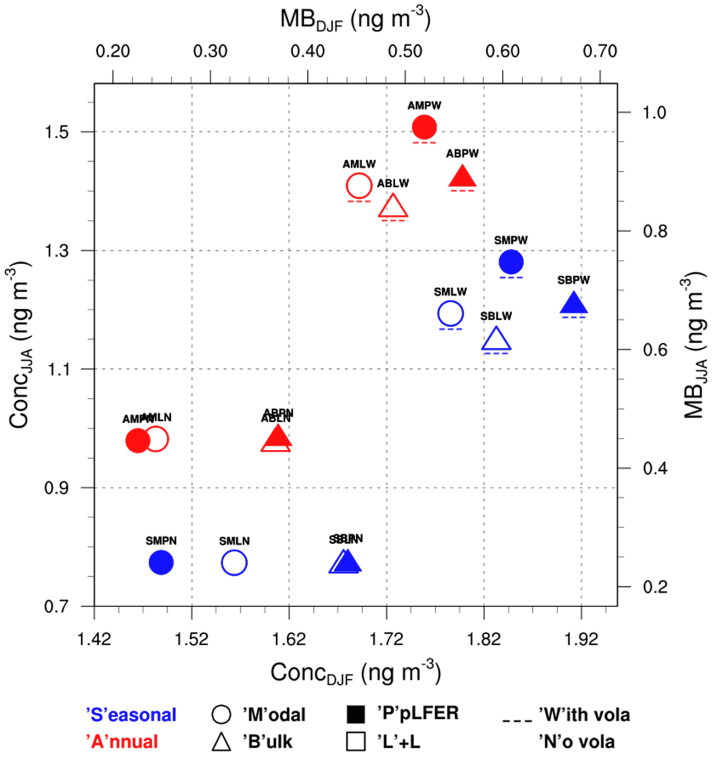

Figure S24. Same as Figure S22, but for FLT concentrations

noticeable differences only in volatilizaton experiments with $\Delta\text{Conc}_{\text{JJA}}$ leading to higher biases (0.027 ng m^{-3}). Similarly, the sign of response due to emission change depends on the interaction with *fac4*, albeit small $\Delta\text{Conc}_{\text{JJA}}$ values in comparison to the others. It is positive if volatilization is accounted for ($\Delta\text{Conc}_{\text{JJA}} = 0.007$ ng m^{-3}) and negative if volatilization is neglected ($\Delta\text{Conc}_{\text{JJA}} = -0.004$ ng m^{-3}).

All experiments in Figure S24b show a consistent positive bias for FLT concentrations in the northern mid-latitudes. The effect of volatilization is positive and relatively stronger than those of other factor changes. ΔConc ranges from 0.121 ng m^{-3} to 0.529 ng m^{-3}, higher in JJA than in DJF by approximately two times. Seasonal emission increases DJF concentrations ($\Delta\text{Conc}_{\text{DJF}} = 0.081$ ng m^{-3}) and substantially decreases JJA concentrations ($\Delta\text{Conc}_{\text{JJA}} = -0.214$ ng m^{-3}). In contrast, the *modal* scheme exhibits a negative concentration response in DJF (hence, less biases), with mean $\Delta\text{Conc}_{\text{DJF}}$ being -0.094 ng m^{-3}, whereas a positive response is apparent in JJA under volatilization scenario ($\Delta\text{Conc}_{\text{DJF}} = -0.055$ ng m^{-3}). Last, *fac3* change brings little to no impact unless volatilization is applied. Here, the ppLFER scheme yields higher concentrations in both seasons by a mean of 0.050 ng m^{-3}.

Benzo[a]pyrene

Figure S25a displays the seasonal concentrations and biases over the Arctic. As shown, all experiments show negative biases in DJF while they show a clear variability of bias in JJA. In particular, most volatilization experiments overestimate the JJA concentrations while all no-volatilization experiments consistently underestimate the concentrations. The mean response to this factor is 1.6×10^{-4} ng m^{-3} in DJF and approximately ten times this value in JJA. Seasonal emission also produces a concentration increase in DJF (on average, by 3.5×10^{-5} ng m^{-3}) but generally brings a decrease in JJA (by -2.2×10^{-4} ng m^{-3}). Changes in *fac2* and *fac3* enhance negative bias in DJF but improve model predictions in JJA by decreasing the concentrations in both seasons. This result suggests the *modal* and ppLFER schemes reduce the atmospheric lifetime of BaP which is attributed to an increase in particulate mass available for oxidation. The degree of both factor effects is similar ($\Delta\text{Conc}_{\text{DJF}} \approx -6\times10^{-5}$ and $\Delta\text{Conc}_{\text{JJA}} \approx -5\times10^{-4}$ ng m^{-3}) which strengthen by at least a factor of two under volatilization scenario.

Similar to the Arctic, all experiments underestimate the concentrations in DJF whereas the sign of JJA bias varies across experiments (Figure S25b). The tendency of volatilization to increase concentrations remains, leading to a positive bias in JJA. In contrast to the Arctic, the mean signal from volatilization is not strongly different between the two seasons nor in comparison with the effects from other factor changes ($\Delta\text{Conc} = 2.7\times10^{-3}$ to 2.6×10^{-2} ng m^{-3}). Seasonal emission contributes to higher concentrations in DJF ($\Delta\text{Conc}_{\text{DJF}} = 2.9\times10^{-3}$ ng m^{-3}) and smaller concentrations in JJA ($\Delta\text{Conc}_{\text{JJA}} = -1.0\times10^{-2}$ ng m^{-3}). The effects of the *modal* and ppLFER schemes are comparable in magnitude but of opposite signs, overall positive for the former (1.0×10^{-3} to 2.6×10^{-3} ng m^{-3}) and negative for the latter (-1.7×10^{-3} to -2.5×10^{-2} ng m^{-3}).

a) Arctic

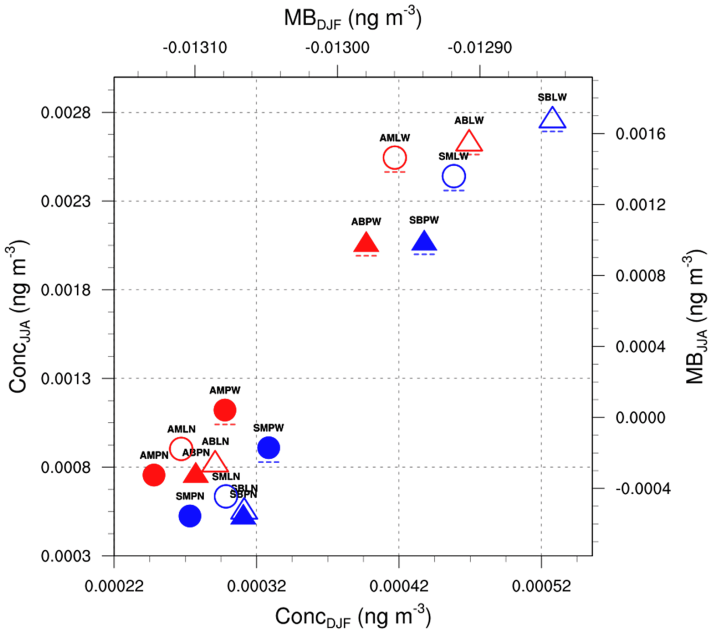

b) NH mid-latitudes

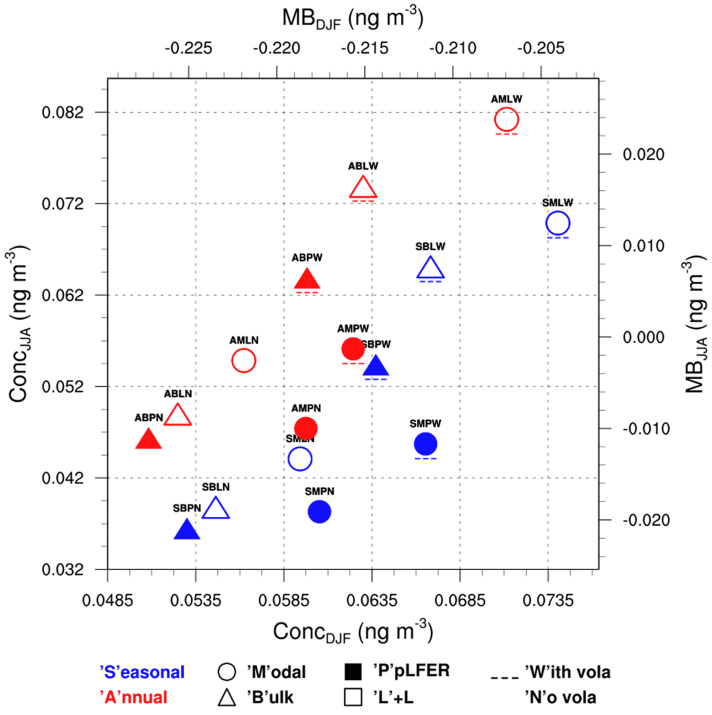

Figure S25. Same as Figure S22, but for BaP concentrations

SVIII Spatial distribution of model bias

In the following, the evaluation of simulated near-surface PAH concentrations against measurements in the Arctic, NH mid-latitudes, and the tropics are discussed. Figures S26-S28 present the distribution of normalized mean bias fraction (NMBF) between model predictions and observations across monitoring stations in the individual region for the time period 2007−2009. As pointed out in Sect. SV, NMBF indicates a model overestimation (by a factor of NMBF +1) or an underestimation (by a factor of 1 − NBMF) when it is positive or negative, respectively. Over the Arctic, the model underestimates PHE and BaP concentrations by at least a factor of two and overestimates FLT by less than a factor of three (Figure S26). The NMBF of PYR varies by location, i.e., negative at E2 and E11 (NMBF = −3.34 and −1.33) and positive at E9 (NMBF = 1.05). This result can be in contrast with the region-based NMBF shown in Table 2, where positive bias (NMBF = 0.06) is produced for the Arctic PYR concentration. Comparing the four species, the degree of bias is consistently higher for BaP where NBMF reaches three orders of magnitude at E2.

For the North American sites (Figure S27a), the model overestimates PHE concentrations with the bias being substantial (NMBF $>$ 15) at three sites (I3, I5, and I6). In contrast, the model systematically underestimates BaP concentrations, particularly at I4 and I7 where the predictions are over a factor of 40 smaller than observations. The degree of NMBF for both species is smaller for the European sites (−5.28 to 4.54 for PHE and −10.85 to 5.15 for BaP) and no systematic bias present (Figure S27b). PYR and FLT concentrations are better simulated than PHE and BaP (except at E5 and E10) with the predictions are overall within a factor of six of observations. It is noted that, for all species, the region-based NMBF (Table 2) is lower than the station-based values as the result of a compensating effect of negative and positive bias amongst the stations clustered in the region. Figure S28 shows that the NMBF values in the tropics are apparently smaller at M5 (NMBF = −0.22 to 0.52), followed by those at M2 (NMBF = −1.36 to −0.67). The model shows underestimation at M1 and M4 (NMBF = −9.26 to −2.50) and overestimation at M3 and M6 (NMBF = 3.81−7.83). The region-based bias is negative for all species (see Table 2 and Figure 5) and is attributed to the monthly concentrations at MI that are much higher than the concentrations at other sites by a factor of 3−170.

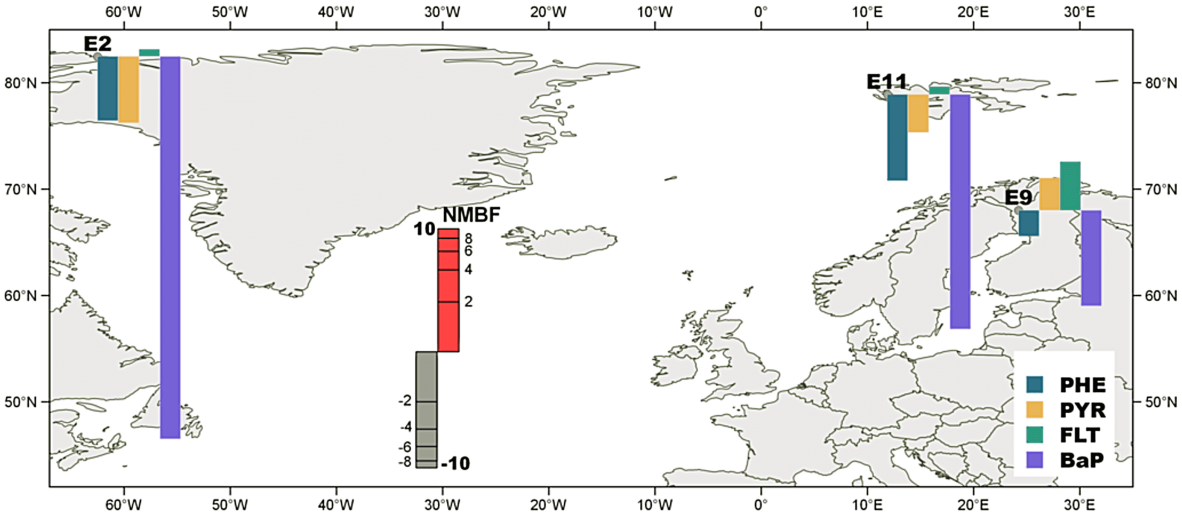

Figure S26. Map of normalized mean bias factor (NMBF) values calculated between simulated and observed mean monthly PAH concentrations for monitoring stations in the Arctic. The logarithmic scale has been used for NMBF.

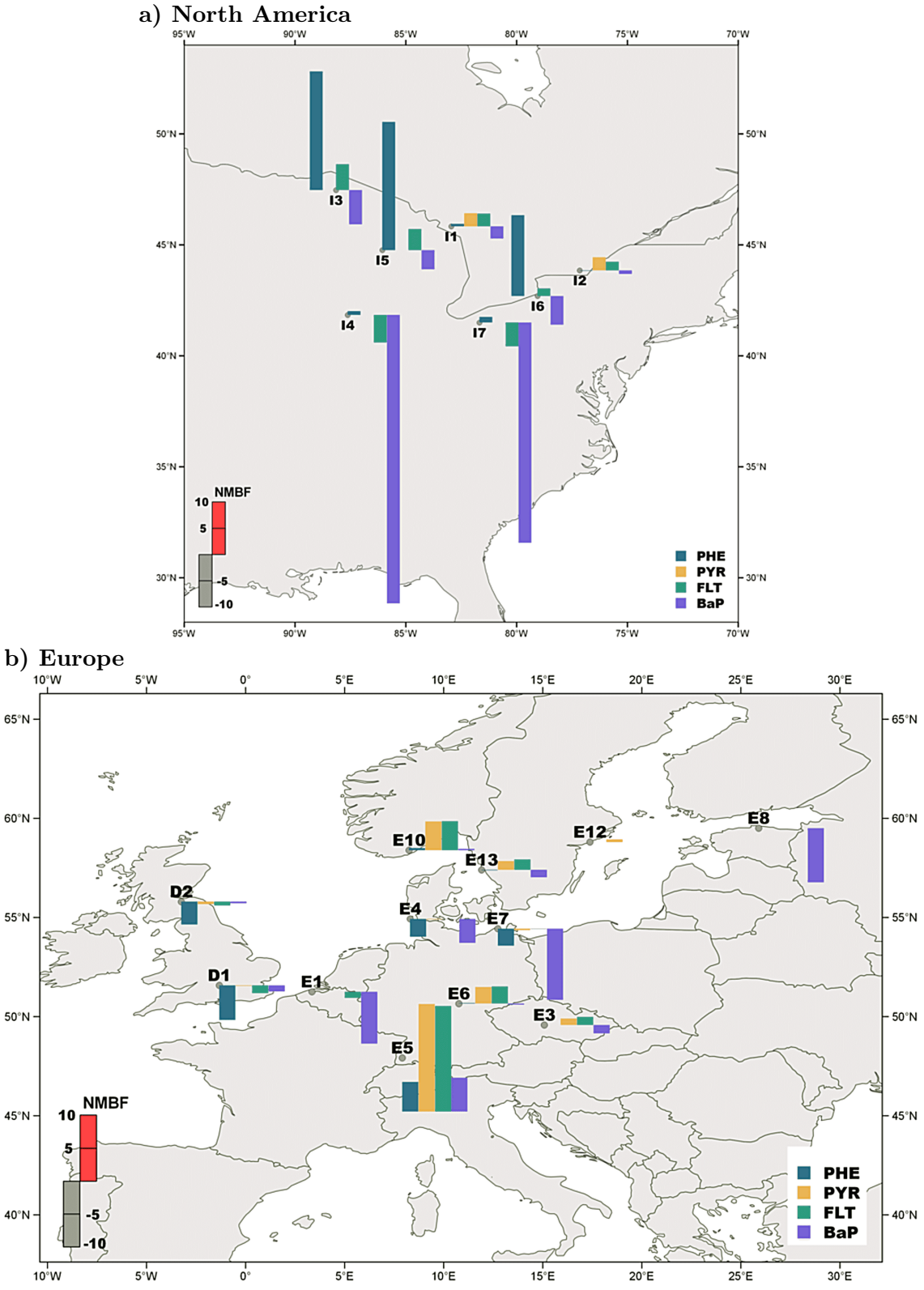

Figure S27. Same as Figure S26 but for monitoring stations in the northern mid-latitudes: (a) North America, and (b) Europe.

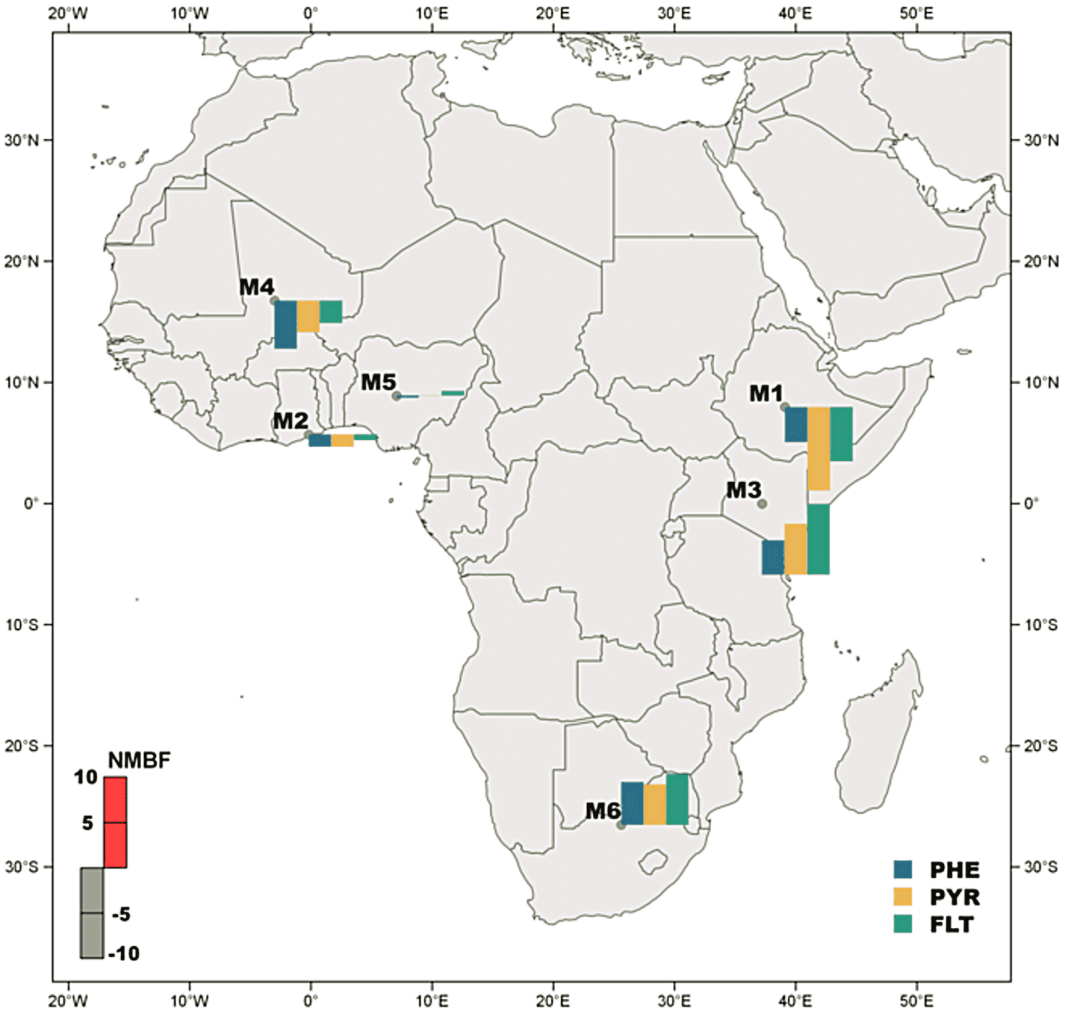

Figure S28. Same as Figure S26 but for monitoring stations in the tropics.

SIX SVOC evaluation: Intermodel comparison

A comparison of simulated PAH concentrations from the new EMAC model (with SVOC submodel) for the year 2007−2009 and from GEOS-Chem model for 2005−2009 (Friedman and Selin, 2012) revealed that both models overall overestimate observed PHE and PYR over mid-latitudes whereas the Arctic concentrations for both species are underestimated by EMAC but overestimated by GEOS-Chem in winter. The discrepancies are more likely to be caused by different emission inventory and by high spatial variability in the emissions which results in changes in PAH concentrations on scales not captured by both GCMs with a grid spacing of >100 km. It is also noteworthy that the simulation carried out with GEOS-Chem differs in complexity to EMAC, that is, the model neglected volatilization and seasonal variation in emissions and applied a dual BC adsorption and OM absorption gas−particle partitioning. Nevertheless, both models systematically underestimate the BaP concentrations over all regions, reflecting a difficulty in modeling the behavior of this species. Model bias is usually larger for the Arctic sites than for the mid-latitude sites and the agreement with observations is more satisfactory in summer. BaP underestimation in remote regions has also been reported in other global modeling studies (Sehili and Lammel, 2007; Shrivastava et al., 2017). Despite uncertainties in the emissions, which seasonality has been taken into account in our simulations, this finding suggests that current models underestimate the role of temperature for the long-range transport of BaP. A GEOS-Chem configuration which neglected heterogeneous oxidations for BaP yielded predicted concentrations higher than measurements over NH mid-latitudes but rather in a good agreement over the Arctic (Friedman and Selin, 2012), suggesting a strong dependence of BaP long-range transport on the temperature sensitivity of particulate-phase oxidation. Similarly, agreement/overprediction of BaP was found using ECHAM5/HAM model (Lammel et al., 2009) when setting $k^{(2)}_{O_3,het}$ to zero (BAPOB scenario; agreement for the Zeppelin station, overestimation for the Alert station). In addition, the latest global BaP modeling study carried out with CAM5 model (Shrivastava et al., 2017) also found that temperature and humidity are important factors to affect heterogeneous oxidation kinetics of BaP and influence the long-range transport. Their default simulation underestimates observed BaP concentrations by approximately 77% whereas the predictions improved when the model assumed that BaP underwent a complete shielding by highly viscous organic aerosols under cool/dry conditions. It is important to understand further the effect of the variation of temperature and humidity on reactive rate constants of the heterogeneous oxidations during the long-range transport. This topic is discussed in details in Mu et al. (2018).

References

Abraham, M. H., Smith, R. E., Luchtefeld, R., Boorem, A. J., Luo, R., and Acree Jr, W. E.: Prediction of solubility of drugs and other compounds in organic solvents, J. Pharm. Sci., 99, 1500–1515, doi:10.1002/jps.21922, URL http://www.sciencedirect.com/science/article/pii/S0022354915327301, 2010.

Ariyasena, T. C. and Poole, C. F.: Determination of descriptors for polycyclic aromatic hydrocarbons and related compounds by chromatographic methods and liquid−liquid partition in totally organic biphasic systems, J. Chromatogr. A, 1361, 240–254, doi:10.1016/j.chroma.2014.08.008, URL http://www.sciencedirect.com/science/article/pii/S0021967314012370, 2014.

Bamford, H. A., Poster, D. L., and Baker, J. E.: Temperature dependence of Henry's law constants of thirteen polycyclic aromatic hydrocarbons between 4°C and 31°C, Environ. Toxicol. Chem., 18, 1905–1912, doi:10.1002/etc.5620180906, URL http://onlinelibrary.wiley.com/doi/10.1002/etc.5620180906/abstract, 1999.

BioHCWin v1.01: Biodegradation Prediction of Petroleum Hydrocarbons v1.01, EPI Suite Version 4.10, URL www2.epa.gov/tsca-screening-tools/epi-suitetm-estimation-program-interface, 2008.

Brubaker, W. W. and Hites, R. A.: OH reaction kinetics of polycyclic aromatic hydrocarbons and polychlorinated dibenzo-p-dioxins and dibenzofurans, J. Phys. Chem. A, 102, 915–921, doi:10.1021/jp9721199, URL http://pubs.acs.org/doi/pdfplus/10.1021/jp9721199, 1998.

Carvalho, A. C., Carvalho, A., Gelpi, I., Barreiro, M., Borrego, C., Miranda, A. I., and Pérez-Muñuzuri, V.: Influence of topography and land use on pollutants dispersion in the Atlantic coast of Iberian Peninsula, Atmos. Environ., 40, 3969–3982, doi:10.1016/j.atmosenv.2006.02.014, URL http://www.sciencedirect.com/science/article/pii/S135223100600207X, 2006.

Chang, J. C. and Hanna, S. R.: Air quality model performance evaluation, Meteorol. Atmos. Phys., 87, 167–196, doi:10.1007/s00703-003-0070-7, URL http://link.springer.com/article/10.1007/s00703-003-0070-7, 2004.

DEFRA: UK Department of Environment, Food and Rural Affairs. Polycyclic Aromatic Hydrocarbons (PAH) data, URL https://uk-air.defra.gov.uk/data/pah-data, 2010.

EBAS NILU: The EBAS atmospheric database, URL http://ebas.nilu.no, 2012.

Finlayson-Pitts, B. J. and Pitts, J. N.: Chemistry of the upper and lower atmosphere: Theory, experiments, and applications, Academic Press, San Diego, URL http://www.sciencedirect.com/science/book/9780122570605, 2000.

Friedman, C. L. and Selin, N. E.: Long-range atmospheric transport of polycyclic aromatic hydrocarbons: global 3-D model analysis including evaluation of Arctic sources, Environ. Sci. Technol., 46, 9501–9510, doi:10.1021/es301904d, URL http://pubs.acs.org/doi/pdfplus/10.1021/es301904d, 2012.

Galarneau, E., Makar, P. A., Zheng, Q., Narayan, J., Zhang, J., Moran, M. D., Bari, M. A., Pathela, S., Chen, A., and Chlumsky, R.: PAH concentrations simulated with the AURAMS-PAH chemical transport model over Canada and the USA, Atmos. Chem. Phys., 14, 4065–4077, doi:10.5194/acp-14-4065-2014, URL http://www.atmos-chem-phys.net/14/4065/2014/, 2014.

Goss, K.-U., Buschmann, J., and Schwarzenbach, R. P.: Determination of the surface sorption properties of talc, different salts, and clay minerals at various relative humidities using adsorption data of a

diverse set of organic vapors, Environ. Toxicol. Chem., 22, 2667–2672, doi:10.1897/03-56, URL http://onlinelibrary.wiley.com/doi/10.1897/03-56/abstract, 2003.

Harner, T. and Bidleman, T. F.: Measurement of octanol−air partition coefficients for polycyclic aromatic hydrocarbons and polychlorinated naphthalenes, J. Chem. Eng. Data, 43, 40–46, doi:10.1021/je970175x, URL http://pubs.acs.org/doi/pdfplus/10.1021/je970175x, 1998.

IADN: Great Lakes Integrated Atmospheric Deposition Network, URL http://ec.gc.ca/data_donnees/STB-AQRD/Toxics/IADN, 2014.

Kamprad, I. and Goss, K.-U.: Systematic investigation of the sorption properties of polyurethane foams for organic vapors, Anal. Chem., 79, 4222–4227, doi:10.1021/ac070265x, URL http://pubs.acs.org/doi/abs/10.1021/ac070265x, 2007.

Klánová, J., Cupr, P., Holoubek, I., Boruvková, J., Přibylová, P., Kareš, R., Kohoutek, J., Dvorská, A., Tomšej, T., and Ocelka, T.: Application of passive sampler for monitoring of POPs in ambient air. VI. Pilot study for development of the monitoring network in the African continent (MONET-AFRICA 2008), RECETOX_TOCOEN 343, RECETOX MU Brno, Czech Republic, 2008.

Kwamena, N.-O. A., Thornton, J. A., and Abbatt, J. P. D.: Kinetics of surface-bound benzo[a]pyrene and ozone on solid organic and salt aerosols, J. Phys. Chem. A, 108, 11 626–11 634, doi:10.1021/jp046161x, URL http://pubs.acs.org/doi/abs/10.1021/jp046161x, 2004.

Lammel, G., Sehili, A. M., Bond, T. C., Feichter, J., and Grassl, H.: Gas/particle partitioning and global distribution of polycyclic aromatic hydrocarbons — A modelling approach, Chemosphere, 76, 98–106, doi:10.1016/j.chemosphere.2009.02.017, URL http://www.sciencedirect.com/science/article/pii/S0045653509001738, 2009.

Lynn, B. H., Healy, R., and Druyan, L. M.: Quantifying the sensitivity of simulated climate change to model configuration, Clim. Change, 92, 275–298, doi:10.1007/s10584-008-9494-x, URL http://link.springer.com/article/10.1007/s10584-008-9494-x, 2009.

Ma, Y.-G., Lei, Y. D., Xiao, H., Wania, F., and Wang, W.-H.: Critical review and recommended values for the physical−chemical property data of 15 polycyclic aromatic hydrocarbons at 25°C, J. Chem. Eng. Data, 55, 819–825, doi:10.1021/je900477x, URL http://pubs.acs.org/doi/pdfplus/10.1021/je900477x, 2010.

Mackay, D., Shiu, W. Y., Ma, K. C., and Lee, S. C.: Handbook of physical−chemical properties and environmental fate for organic chemicals, vol. I of *Introduction and Hydrocarbons*, Taylor & Francis, 2nd edn., URL http://books.google.de/books?id=22zhOfXJ444C, 2006.

Mintz, C., Burton, K., Ladlie, T., Clark, M., Acree Jr, W. E., and Abraham, M. H.: Enthalpy of solvation correlations for gaseous solutes dissolved in dibutyl ether and ethyl acetate, Thermochim. Acta, 470, 67–76, doi:10.1016/j.tca.2008.02.001, URL http://www.sciencedirect.com/science/article/pii/S0040603108000403, 2008.

Mu, Q., Shiraiwa, M., Octaviani, M., Ma, N., Ding, A., Su, H., Lammel, G., Pöschl, U., and Cheng, Y.: Temperature effect on phase state and reactivity controls atmospheric multiphase chemistry and transport of PAHs, Sci. Adv., 4, doi:10.1126/sciadv.aap7314, URL http://advances.sciencemag.org/content/4/3/eaap7314.abstract, 2018.

Odabasi, M., Cetin, E., and Sofuoglu, A.: Determination of octanol−air partition coefficients and supercooled liquid vapor pressures of PAHs as a function of temperature: Application to gas−particle partitioning in an urban atmosphere, Atmos. Environ., 40, 6615–6625, doi:10.1016/j.atmosenv.2006.05.051, URL http://www.sciencedirect.com/science/article/pii/S1352231006005401, 2006.

Park, K. S., Sims, R. C., Dupont, R. R., Doucette, W. J., and Matthews, J. E.: Fate of PAH compounds in two soil types: Influence of volatilization, abiotic loss and biological activity, Environ. Toxicol. Chem., 9, 187–195, doi:10.1002/etc.5620090208, URL http://onlinelibrary.wiley.com/doi/10.1002/etc.5620090208/abstract, 1990.

Perraudin, E., Budzinski, H., and Villenave, E.: Kinetic study of the reactions of ozone with polycyclic aromatic hydrocarbons adsorbed on atmospheric model particles, J. Atmos. Chem., 56, 57–82, doi:10.1007/s10874-006-9042-x, URL http://link.springer.com/article/10.1007/s10874-006-9042-x, 2007.

Romero, R., Ramis, C., and Alonso, S.: Numerical simulation of an extreme rainfall event in Catalonia: Role of orography and evaporation from the sea, Q. J. Roy. Meteor. Soc., 123, 537–559, doi:10.1002/qj.49712353902, URL http://onlinelibrary.wiley.com/doi/10.1002/qj.49712353902/abstract, 1997.

Roth, C. M., Goss, K.-U., and Schwarzenbach, R. P.: Sorption of a diverse set of organic vapors to diesel soot and road tunnel aerosols, Environ. Sci. Technol., 39, 6632–6637, doi:10.1021/es049204w, URL http://pubs.acs.org/doi/pdfplus/10.1021/es049204w, 2005.

Roux, M. V., Temprado, M., Chickos, J. S., and Nagano, Y.: Critically evaluated thermochemical properties of polycyclic aromatic hydrocarbons, J. Phys. Chem. Ref. Data, 37, 1855–1996, doi:10.1063/1.2955570, URL http://scitation.aip.org/content/aip/journal/jpcrd/37/4/10.1063/1.2955570, 2008.

Sehili, A. M. and Lammel, G.: Global fate and distribution of polycyclic aromatic hydrocarbons emitted from Europe and Russia, Atmos. Environ., 41, 8301–8315, doi:10.1016/j.atmosenv.2007.06.050, URL http://www.sciencedirect.com/science/article/pii/S1352231007005833, 2007.

Shrivastava, M., Lou, S., Zelenyuk, A., Easter, R. C., Corley, R. A., Thrall, B. D., Rasch, P. J., Fast, J. D., Massey Simonich, S. L., Shen, H., and Tao, S.: Global long-range transport and lung cancer risk from polycyclic aromatic hydrocarbons shielded by coatings of organic aerosol, Proc. Natl. Acad. Sci., 114, 1246–1251, doi:10.1073/pnas.1618475114, URL http://www.pnas.org/content/114/6/1246.abstract, 2017.

Sprunger, L., Proctor, A., Acree, W. E., and Abraham, M. H.: Characterization of the sorption of gaseous and organic solutes onto polydimethyl siloxane solid-phase microextraction surfaces using the Abraham model, J. Chromatogr. A, 1175, 162–173, doi:10.1016/j.chroma.2007.10.058, URL http://www.sciencedirect.com/science/article/pii/S0021967307018195, 2007.

Stein, U. and Alpert, P.: Factor separation in numerical simulations, J. Atmos. Sci., 50, 2107–2115, doi:10.1175/1520-0469(1993)050<2107:FSINS>2.0.CO;2, URL http://journals.ametsoc.org/doi/abs/10.1175/1520-0469(1993)050%3C2107%3AFSINS%3E2.0.CO%3B2, 1993.

ten Hulscher, T. E. M., Van Der Velde, L. E., and Bruggeman, W. A.: Temperature dependence of Henry's law constants for selected chlorobenzenes, polychlorinated biphenyls and polycyclic aromatic hydrocarbons, Environ. Toxicol. Chem., 11, 1595–1603, doi:10.1002/etc.5620111109, URL http://onlinelibrary.wiley.com/doi/10.1002/etc.5620111109/abstract, 1992.

Torma, C. and Giorgi, F.: Assessing the contribution of different factors in regional climate model projections using the factor separation method, Atmos. Sci. Lett., 15, 239–244, doi:10.1002/asl2.491, URL http://onlinelibrary.wiley.com/doi/10.1002/asl2.491/abstract, 2014.

Wasik, S., Miller, M., Tewari, Y., May, W., Sonnefeld, W., De Voe, H., and Zoller, W.: Determination of the vapor pressure, aqueous solubility, and octanol/water partition coefficient of hydrophobic substances by coupled generator column/liquid chromatographic methods, in: Residue Reviews,

edited by Gunther, F. A. and Gunther, J. D., vol. 85 of *Residue Reviews*, pp. 29–42, Springer New York, doi:10.1007/978-1-4612-5462-1_4, 1983.

Yamasaki, H., Kuwata, K., and Kuge, Y.: Determination of vapor pressure of polycyclic aromatic hydrocarbons in the supercooled liquid phase and their adsorption on airborne particulate matter, Nippon Kagaku Kaishi, 1984, 1324–1329, doi:10.1246/nikkashi.1984.1324, URL https://www.jstage.jst.go.jp/article/nikkashi1972/1984/8/1984_8_1324/_article, 1984.

Yu, S., Eder, B., Dennis, R., Chu, S.-H., and Schwartz, S. E.: New unbiased symmetric metrics for evaluation of air quality models, Atmos. Sci. Lett., 7, 26–34, doi:10.1002/asl.125, URL http://onlinelibrary.wiley.com/doi/10.1002/asl.125/pdf, 2006.